ΠΑΝΕΠΙΣΤΗΜΙΟ ΘΕΣΣΑΛΙΑΣ

ΣΧΟΛΗ ΘΕΤΙΚΩΝ ΕΠΙΣΤΗΜΩΝ

ΔΙΑΤΜΗΜΑΤΙΚΟ ΠΡΟΓΡΑΜΜΑ ΜΕΤΑΠΤΥΧΙΑΚΩΝ ΣΠΟΥΔΩΝ

ΠΛΗΡΟΦΟΡΙΚΗ ΚΑΙ ΥΠΟΛΟΓΙΣΤΙΚΗ ΒΙΟΙΑΤΡΙΚΗ

Επεξεργασία και ανάλυση φάσματος ηλιακών ραδιοεκπομπών του ηλιακού ραδιοφασματογράφου ΑΡΤΕΜΙΣ IV

ΣΜΑΝΗΣ ΘΕΟΦΑΝΗΣ

ΔΙΠΛΩΜΑΤΙΚΗ ΕΡΓΑΣΙΑ

Επιβλέπων

ΔΕΛΗΜΠΑΣΗΣ ΚΩΝ/ΝΟΣ

Λαμία 20 Ιουλίου 2019

UNIVERSITY OF THESSALY

SCHOOL OF SCIENCE

INFORMATICS AND COMPUTATIONAL BIOMEDICINE

Software development for data import and image processing of the ARTEMIS-IV J.L.STEINBERG solar spectrometer

SMANIS FANIS

Master thesis

Supervisor

DELIMBASIS KON/NOS

Lamia

20/6/2019

ΠΑΝΕΠΙΣΤΗΜΙΟ ΘΕΣΣΑΛΙΑΣ

ΣΧΟΛΗ ΘΕΤΙΚΩΝ ΕΠΙΣΤΗΜΩΝ

ΔΙΑΤΜΗΜΑΤΙΚΟ ΜΕΤΑΠΤΥΧΙΑΚΟ ΠΡΟΓΡΑΜΜΑ ΠΛΗΡΟΦΟΡΙΚΗ ΚΑΙ ΥΠΟΛΟΓΙΣΤΙΚΗ ΒΙΟΙΑΤΡΙΚΗ

ΚΑΤΕΥΘΥΝΣΗ

«ΥΠΟΛΟΓΙΣΤΙΚΗ ΙΑΤΡΙΚΗ ΚΑΙ ΒΙΟΛΟΓΙΑ»

Επεξεργασία και ανάλυση φάσματος ηλιακών ραδιοεκπομπών του ηλιακού ραδιοφασματογράφου ΑΡΤΕΜΙΣ IV

ΣΜΑΝΗΣ ΘΕΟΦΑΝΗΣ

ΔΙΠΛΩΜΑΤΙΚΗ ΕΡΓΑΣΙΑ

Επιβλέπων

ΔΕΛΗΜΠΑΣΗΣ ΚΩΝ/ΝΟΣ

Λαμία 20 Ιουλίου 2019

«Υπεύθυνη Δήλωση μη λογοκλοπής και ανάληψης προσωπικής ευθύνης»

Με πλήρη επίγνωση των συνεπειών του νόμου περί πνευματικών δικαιωμάτων, και γνωρίζοντας τις συνέπειες της λογοκλοπής, δηλώνω υπεύθυνα και ενυπογράφως ότι η παρούσα εργασία με τίτλο [«τίτλος εργασίας»] αποτελεί προϊόν αυστηρά προσωπικής εργασίας και όλες οι πηγές από τις οποίες χρησιμοποίησα δεδομένα, ιδέες, φράσεις, προτάσεις ή λέξεις, είτε επακριβώς (όπως υπάρχουν στο πρωτότυπο ή μεταφρασμένες) είτε με παράφραση, έχουν δηλωθεί κατάλληλα και ευδιάκριτα στο κείμενο με την κατάλληλη παραπομπή και η σχετική αναφορά περιλαμβάνεται στο τμήμα των βιβλιογραφικών αναφορών με πλήρη περιγραφή. Αναλαμβάνω πλήρως, ατομικά και προσωπικά, όλες τις νομικές και διοικητικές συνέπειες που δύναται να προκύψουν στην περίπτωση κατά την οποία αποδειχθεί, διαχρονικά, ότι η εργασία αυτή ή τμήμα της δεν μου ανήκει διότι είναι προϊόν λογοκλοπής.

Ο ΔΗΛΩΝ

Ημερομηνία 20/6/2019

Υπογραφή

Τριμελής Επιτροπή:

Ονοματεπώνυμο, ΕΠΙΒΛΕΠΩΝ - ΔΕΛΗΜΠΑΣΗΣ ΚΩΝ/ΝΟΣ

Ονοματεπώνυμο, ΣΑΝΔΑΛΙΔΗΣ ΧΑΡΙΛΑΟΣ

Ονοματεπώνυμο, ΚΑΚΑΡΟΥΝΤΑΣ ΑΘΑΝΑΣΙΟΣ

Abstract

The processing and analysis of the solar spectrum for the detection of radio bursts, is of increased importance for solar astronomy, as it affects many aspects of human activity (e.g. Tele communications).

This thesis introduces new methods of importing, and processing data from the radio telescope Artemis IV and its spectrographs. The acousto-optic receiver of the ARTEMIS solar radio spectrograph (now the Jean-Louis Steinberg spectrograph, situated at Thermopiles, Fthiotida, Greece) provides dynamic spectra with a time resolution of 10 ms and a 1.4 MHz bandwidth in the frequency range of 270 to 450 MHz.

As a first step, the format of the raw data of the spectrograph's output files was studied and the appropriate software functions were constructed to import the data into the Matlab programming environment and generate the images of the dynamic solar spectrum. Furthermore, two novel image processing algorithms were designed and developed, in order to preprocess the images of the dynamic solar spectrum. More specifically, the first image processing algorithm is based on the convolution of the line profile of the image with an appropriate 1D kernel, in order to detect terrestrial radio sources, followed by morphological processing to remove them. The 2nd proposed method is based on a directional Fourier-based image processing to remove artificial radio sources from the dynamic spectrum.

Results are presented for a small number of dynamic spectrum images that contain solar events of interest. The preprocessed images show enhanced visibility of all types of solar radio bursts.

1. INTRODUCTION

1.1. The Sun

The Earth's mother-star is a type G2 star and has an average distance from earth of 1A.U. = 149.598.000±250 Km. This distance equals to approximately 215 suns radius, equivalently the light takes 8 min 18.9 sec to reach planet earth. Sun's radius is 696000 Km, times 109 earths radius and the mass of $1.989 \cdot 10^{30}$ Kgr, whereas its density is equal to 0.26 earth's density.

Fig.1 Sun with sunspots and limb darkening as seen in visible light with solar filter.

[https://en.wikipedia.org/wiki/Sun]

The sun' gravitational force is 28 times bigger than earth's and it is approximately $g=275\ m/s^2$. Sun has a declination of $82^o 45'$ from the vertical axis and spins from east to west in 25.38 days in his equator and nearly 34 days around his pole. The escape velocity is 617.7 Km/sec, 56 times bigger than earth's, which is 11.2 Km/sec.

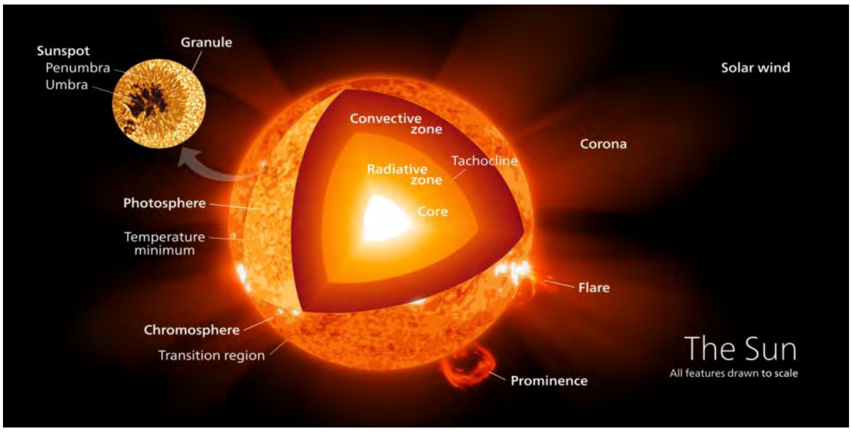

Fig.2 The structure of the Sun
[https://en.wikipedia.org/wiki/Sun]

Sun is a very big mass of gas which is divided into the internal part and the solar atmosphere. The following figure shows the variation from the center of the sun towards its surface of the following quantities [1]: *Temperature* (lower left), *Angular speed of rotation* (upper right), *Density and composition* (lower right) and *Energy flux*, that increases almost in a linear manner towards the solar surface.

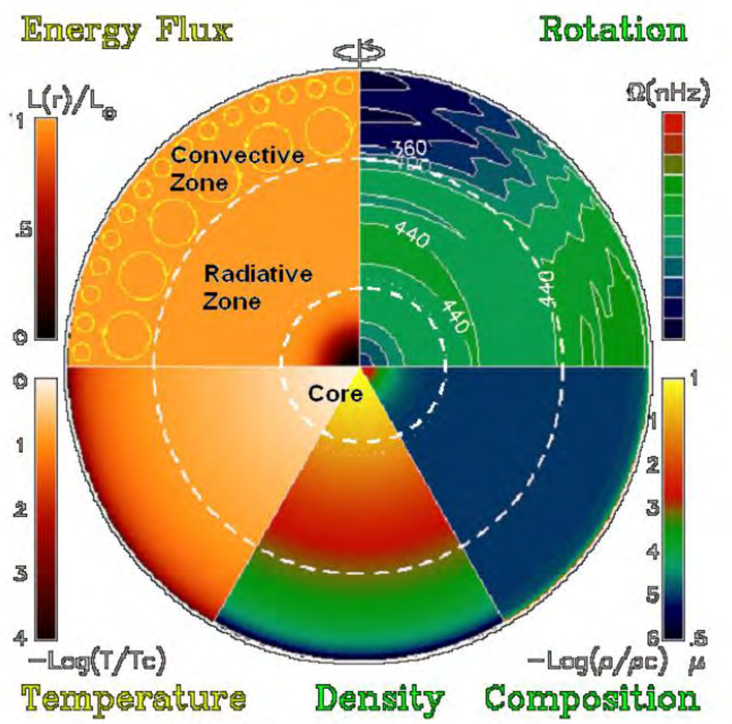

Fig.3. Suns internal areas
https://en.wikipedia.org/wiki/Sun#Atmosphere

The Sun's internal consists of the core, the radiative zone and the convective zone.

- ***Core*** is the area that thermonuclear reaction take place that produce its energy, which is radiated to our solar system. It has a temperature at $14\cdot10^{6}$ °K, pressure at $2\cdot10^{11}$ atm and density of 135 gr/cm^{3}.The energy that is produced is transmitted by radiation and needs 10^{7} years to run $500\cdot10^{6}$m
- ***The radiative zone*** is an area nearly 0.6 suns radius with an average temperature at $2.5\cdot10^{6}$ °K and 1 gr/cm^{3} density that also transmits radiation.
- ***The convective zone*** is the last inner sun's zone, within which heated mass currents moving upwards and eventually cool down after reaching high altitude and decentigrate at lower levels. The temperature of the convective zone is about $2\cdot10^{6}$ °K and the density decreases at 0.1 gr/cm^{3}.

The Solar Atmosphere.

The solar atmosphere consists of the photosphere, the chromosphere, the transfer area and the corona [2]. The temperature and particle density as a function of the height of the sun's atmosphere is shown in the Figure below.

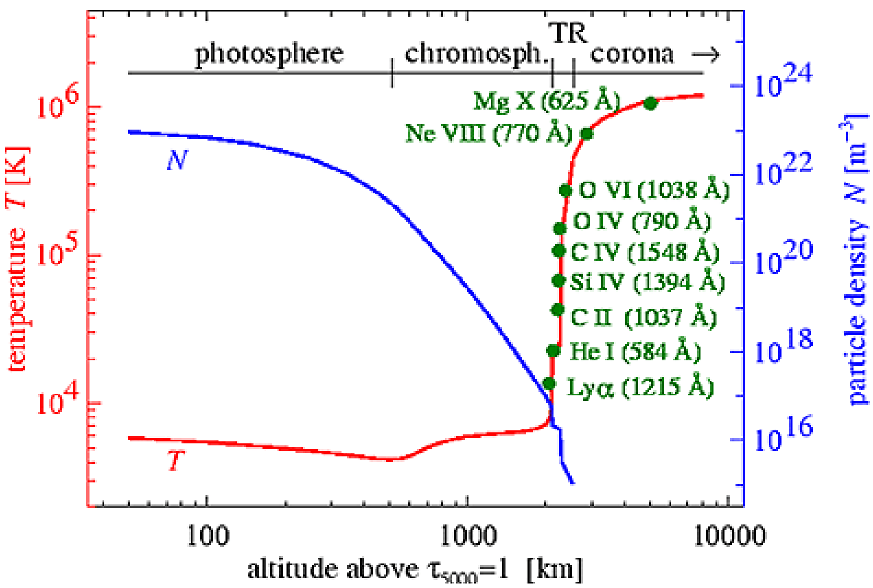

Fig.4. Schematic temperature and particle density through the solar chromosphere and transition region

https://en.wikipedia.org/wiki/Sun#Atmosphere

- ***Photosphere*** extends from 400 Km to 700000 Km and emits the visual band of the continuous solar optical spectrum and it is the visible sun's surface. Its temperature is 5900 ^{o}K , its pressure equals 1% of the earth's atmospheric pressure and its density is 10^{-7} gr/cm^{3}. Inside the photosphere we can see granules and sunspots.

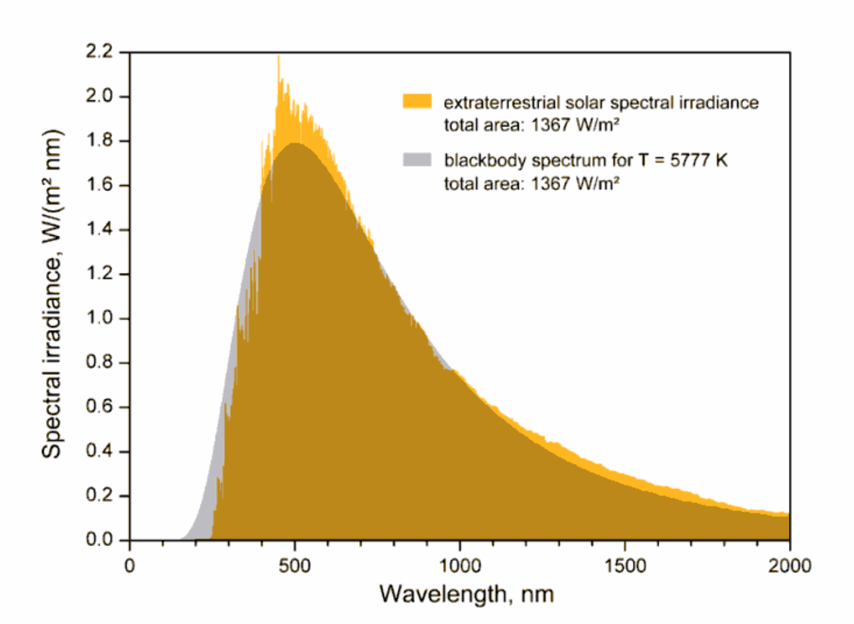

Fig.5.
The effective temperature, or black body temperature, of the Sun (5,777 K) is the temperature a black body of the same size must have to yield the same total emissive power.
https://en.wikipedia.org/wiki/Sun#Atmosphere

- ***Granules*** are the higher spots of the up going layers of heat that return to the lower layers in about 10 min with a speed of approximately 500 m/sec and temperature at 200^{o} K, which is the highest in the photosphere area and 400 Km width.
- ***Sunspots*** are deep curves in depth of 800 Km and temperature at 4600^{o} K that create the illusion of dark areas inside the much hotter photosphere, which follow a periodic solar circle with 11 years of appearance.

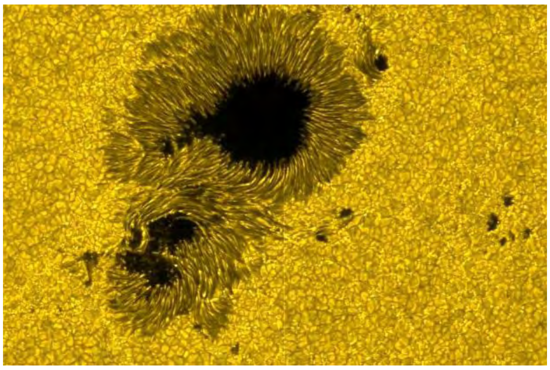

Fig.6. Visible light photograph of sunspot, 13 December 2006

https://en.wikipedia.org/wiki/Sun#Atmosphere

The Chromosphere

Chromosphere expands to 2 Mm high above the photosphere and its density is about 1000-10000 times smaller than the photosphere density. The temperature initially increases slowly from 6000^o K and then increases rapidly up to 25000^o K. Inside the chromosphere we can observe super granulations with edges that provide the chromospheric network and also fibrils. The chromospheric network can be seen in the chromospheric lines and also in radio waves with wavelength at cm. In this network we can observe a concentration of magnetic lines with magnitude of 100 mT, while the average magnetic field magnitude is only 3 mT. Prominences, specular, flares, as well as chromospheric eruptions can be also observed [2].

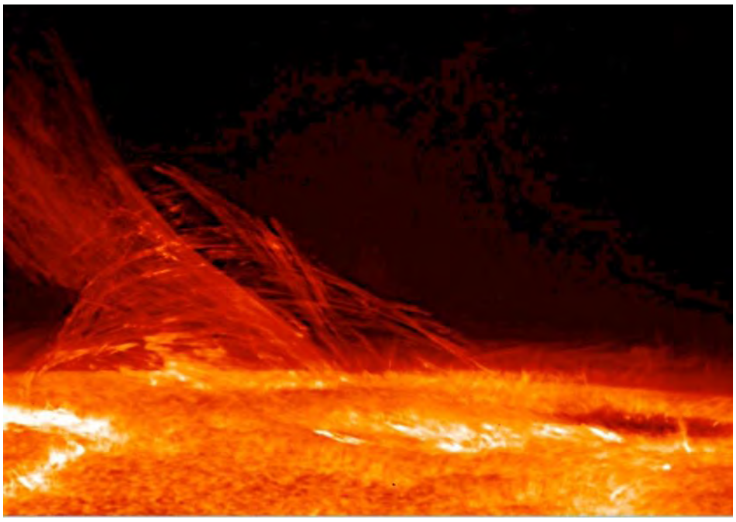

Fig.7. Taken by Hinode's Solar Optical Telescope on 12 January 2007, this image of the Sun reveals the filamentary nature of the plasma connecting regions of different magnetic polarity.

https://en.wikipedia.org/wiki/Sun#Atmosphere

The transfer area

This area is located just above the chromosphere and has a width of some hundreds Km. The main characteristic is a very rapid increase of temperature from $25 \cdot 10^3$ ^oK to 10^6 ^{o} K. Due to the increasing temperature, the density decreases 100 times. The other characteristics differ over super-granulations and chromospheric network, because of the strong magnetic field. This magnetic field in the network is vertical and reduces with high. The elements of the network can be well observed in the spectrum lines of Ne VII. [2]

The Corona

Corona is an extremely hot and thin layer of the dynamic solar atmosphere. It begins just after the transfer area and including the solar wind, it expands reaching the planets and furthermore the solar system's final frontier, the oart cloud.

Fig.8. During a total solar eclipse, the solar corona can be seen with the naked eye, during the brief period of totality.
https://en.wikipedia.org/wiki/Sun#Atmosphere

The structure, the flow of energy inside it and the dynamic motions are due to the solar magnetic field. In order to study the corona, the visible light frequencies are being used during solar eclipses or a coronagraph in various emission spectrum lines, such as EUV, x rays and radio waves. The images that we take with x rays show great unbalance which is constantly changing.

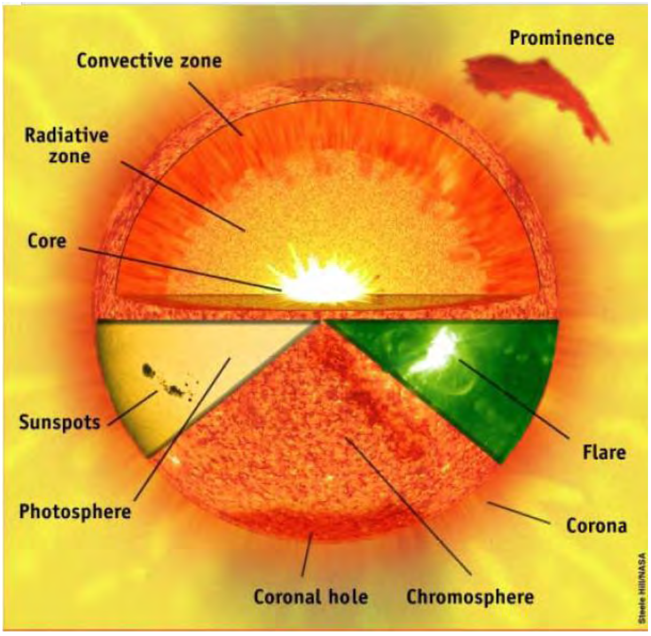

Fig.10. The components of the Sun

[https://en.wikipedia.org/wiki/Sun]

We can point out different areas with intensive radiation field which are combined with the burst loops made by the magnetic field. When we observe the corona using radio waves the image that we take depends on the frequency of observation and differs from time to time according to the time scale that we use. [2]

The corona holes, are stematic areas where the electric density is much lower, approximately 10 times, than the density of nearby areas. In these regions lower temperatures are also measured. The corona holes are being observed by X rays, He lines and radio waves. The magnetic field is monopolic with an axes through the middle of its center and has a declination near the edges. Nearly all of the magnetic lines that reach the outer parts of the solar stema and the interplanetary space, have their basis and its origins inside the corona's holes. Also a big percentage of the solar wind has its origins inside the corona's holes. At the minimum of solar activity we can observe two vast polar corona holes. The exact position of the corona holes can be calculated by the bipolar areas of the sun spots and the magnetic equator of the Sun. [2]

Solar Magnetic Field

The instabilities of the solar magnetic field are the reason of the most of the exquisite phenomena that take place in sun's surface and atmosphere such as sunspots, flares , bursts , Coronal Mass Ejections(CME) , and radiation rays in the visual , ultraviolet , infrared , x rays and radio wave length as well as the heating of corona. It is possible that the magnetic field is made by the interaction of the hot ascending with the cold descending transport flows, which move continuously in the transfer area and are combined with the spinning speed of the sphere, which is differential according to the depth and the heliographic latitude. The active regions create the primary appearance of the bipolar magnetic field the loop of the magnetic dynamic lines of differential spinning and the form of the active regions. [2]

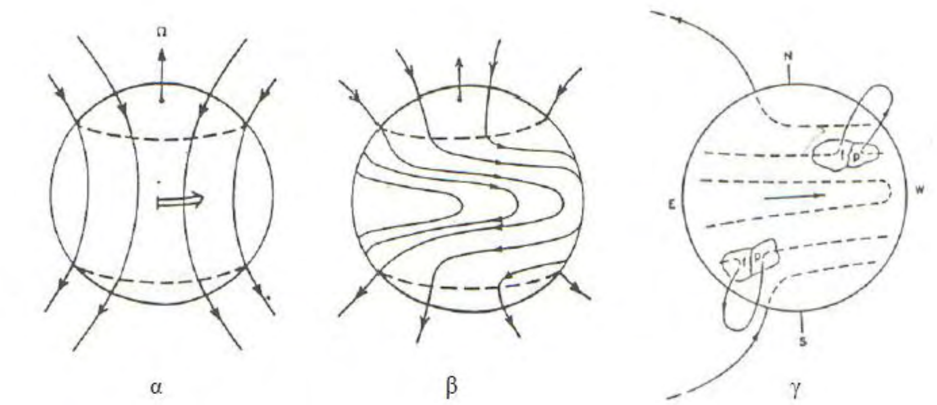

Fig.11. Dynamic lines of the solar magnetic field.

[https://en.Wikipedia.org/wiki/Sun]

The calm Sun

There are only few times that the sun is calm and there are no observation on the surface or at the electromagnetic spectrum. The brilliance B is the degree of brightness of a star. The magnitude of an astronomical object is now defined as the negative logarithm of the brightness. (A decrease of one magnitude represents an increase in brightness of 2.512 times. A star with an apparent magnitude of six is barely visible to the naked eye). The Suns brilliance equals -26.74. Also the density of flow compared to the wavelength of radiation can be seen in the next diagrams when the Sun is calm and also when it is disturbed.

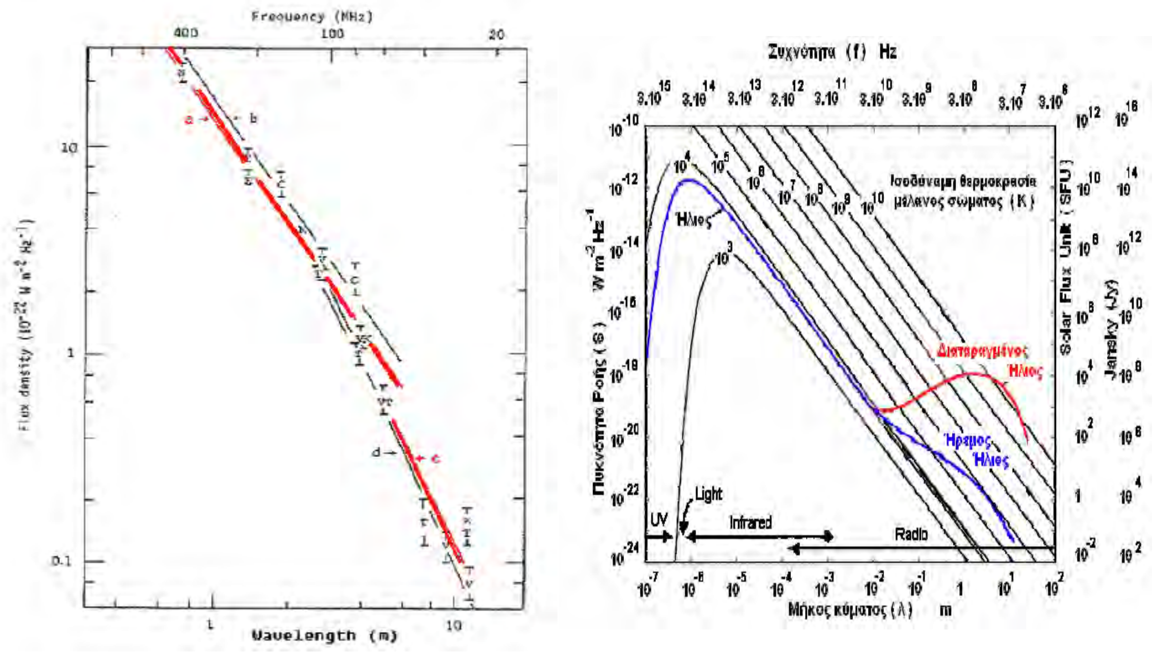

Fig.12. *[https://en.wikipedia.org/wiki/Sun]*

The Sun appears to be bigger when is been observed by radio-telescopes than with optical telescopes. In the next diagram we can see that Sun looks bigger in higher wavelength, using various data from radio heliographs in different wavelengths. If the sun was totally calm, the iso - phote curves would be concentric circles. However this is a rare thing to observe as you can see below. [2]

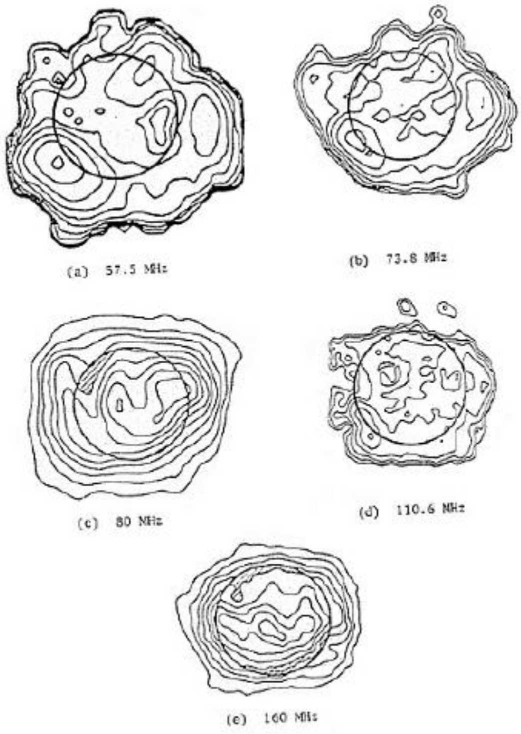

Fig.13. Sun's image in differential frequency iso-photes. The circle shows the visual solar disk (Sheridan and McLean, 1985). [3] [https://en.wikipedia.org/wiki/Sun]

The active Sun

Radio bursts can originate from our galaxy or any other galaxy of the universe as shown in [55]. Fast Radio Bursts (FRBs) are isolated with dispersion measure (DM) of order 10^3 pc /cm^{-3}. However, the sun is the strongest emitter of radio bursts. Solar activity is generated and controlled by the magnetic field, due to

i) The active regions with the sunspots, the flares, the threads as well as the densities and the magnetic field's differential behaviors.
ii) The eleventh year circle of the solar activity.
iii) The solar flares and the relevant phenomena such as CME's, radio bursts and explosive protrusions.

Sunspots are temporary phenomena on the Sun's photosphere that appear as spots darker than the surrounding areas. They are regions of reduced surface temperature caused by concentrations of magnetic field flux that inhibit convection. Sunspots usually appear in pairs of opposite magnetic polarity. Their number varies according to the approximately 11-year solar cycle. [7]

A solar flare is a sudden flash of increased brightness on the Sun, usually observed near its surface and in close proximity to a sunspot group. Powerful flares are often, but not always, accompanied by a coronal mass ejection. Even the most powerful flares are barely detectable in the total solar irradiance (the "solar constant"). [5]

The solar cycle or solar magnetic activity cycle is the nearly periodic 11-year change in the Sun's activity (including changes in the levels of solar radiation and ejection of solar material) and appearance (changes in the number and size of sunspots, flares, and other manifestations).[5]

A coronal mass ejection (CME) is a significant release of plasma and accompanying magnetic field from the solar corona. They often follow solar flares and are normally present during a solar prominence eruption. The plasma is released into the solar wind and can be observed in coronagraph imagery. [8][9][10]

Types of radio bursts:

In the literature five different types of radio bursts have been reported.

- ***Type I :***

  CHARACTERISTICS: short, narrow-bandwidth bursts. Usually occur in large numbers with underlying continuum.

  DURATION: single burst: ~ 1 second,
  Storm: hours - days

  FREQUENCY RANGE: 80 – 200 MHz

  ASSOCIATED PHENOMENA: Active regions, flares, eruptive prominences. [62]

- ***Type II:***

  CHARACTERISTICS: Slow frequency drift bursts. Usually accompanied by a (usually stronger intensity) second harmonic.

  DURATION: 3- 30 minutes

  FREQUENCY RANGE: Fundamental: 20 – 150 MHz

ASSOCIATED PHENOMENA: Flares, proton emission,
Magneto-hydrodynamic shockwaves.
[4],[17],[23],[38],

- ***Type III:***

  CHARACTERISTICS: Fast frequency drift bursts. Can occur singularly, in groups, or storms (often with under lying continuum). Can be accompanied by a second harmonic

  DURATION: Single burst: 1 - 3 seconds
  Group: 1 -5 minutes
  Storm: minutes – hours

  FREQUENCY RANGE: 10 kHz – 1 GHz

  ASSOCIATED PHENOMENA: Active regions, flares. [4],[44]

- ***Type IV:***

  CHARACTERISTICS:

  Stationary Type IV: Broadband continuum with fine structure

  DURATION: Hours – days

  FREQUENCY RANGE: 20 MHz – 2 GHz

  ASSOCIATED PHENOMENA: Flares, proton emission.

  CHARACTERISTICS:

  Moving Type IV: Broadband, slow frequency drift, smooth continuum.

  DURATION: 30 – 2 hours

  FREQUENCY RANGE: 20 – 400 MHz

  ASSOCIATED PHENOMENA: Eruptive prominences, magneto hydrodynamic shockwaves. [17],[45]

  CHARACTERISTICS:

  Flare Continua: Broadband, smooth continuum.

  DURATION: 3 – 45 minutes

  FREQUENCY RANGE: 25 – 200 MHz

  ASSOCIATED PHENOMENA: Flares, proton emission

- ***Type V:***

  CHARACTERISTICS: Smooth, short-lived continuum.

  Follows some type III bursts.

  Never occur in isolation.

  DURATION: 1-3 minutes

  FREQUENCY RANGE: 10 - 200 MHz

  ASSOCIATED PHENOMENA: Same as type III bursts

  [63],[64]

1.2. Solar physics of radio bursts

Understanding the Sun is not only important in the context of Physics and Astrophysics, but also for our daily life. This is not only because the Sun provides us with light and energy, but also because it affects us in more subtle, yet important, ways that came to our knowledge just a few decades ago. In addition to the electromagnetic radiation, the Sun emits a constant flow of plasma, the solar wind, which is the supersonic hydrodynamic expansion of its outer layer, the corona. Moreover, huge amounts of energy can be stored in the magnetic field of the solar atmosphere, to be released in the course of huge eruptions: flares and Coronal Mass Ejections (CMEs). Flares produce intense electromagnetic radiation at radio wavelengths, in the ultraviolet (UV) and in X-rays, while CMEs, propagating to the Earth's orbit and beyond, carry plasma and magnetic field. Both flares and CMEs can accelerate electrons and protons to high energies. The effects in the terrestrial environment are important, sometimes severe: ionospheric disturbances affecting radio communications and GPS systems; magnetospheric disturbances affecting power lines and all sorts of electric and electronic systems and occasionally satellites; energetic particles posing a radiation threat to astronauts. Thus the development of the space weather science with the ultimate goal of forecasting solar phenomena that adversely affect human life and activities. Communication and GPS receivers are the most sensitive equipment to solar activity. In [54],[60] the effect of the solar activity of 6th December 2006 on GPS receivers is studied by measuring the carrier-to-noise ratio in order to find the interference of the sun's radio burst. The obtained results give a serious ground to revise the role played by space weather factors in operation of modern satellite systems and to take these factors into account more carefully, when such systems are designed and exploited.

Since flares and CMEs are sporadic phenomena whose timing and manifestations are at present not predictable, their detection requires continuous monitoring, as opposed to pre-planned observations that are the rule in other domains of astrophysics. Although regular observations of the sun are being performed for decades in some observatories, it was in the late 60's that a world-wide network of observatories started developing for the continuous monitoring of the solar activity, providing observations first in the optical and then in the radio domain, both accessible from the ground. In our days, ground based observations are supplemented by a large number of space missions, providing information in spectral ranges not accessible from the ground (UV, X-rays, decametric and longer radio wavelengths), as well as measurements of energetic particles and the solar wind. The value of these instruments goes far beyond patrol, as the information they have been providing has deepened our understanding of the physics of the Sun, including the physics of solar flares and CMEs.

Measurements in the radio band of the electromagnetic spectrum (decimetric and longer wavelengths) provide important information on solar energetic phenomena. As the accelerated electrons move upwards in the corona, they excite Langmuir waves which, in turn, produce electromagnetic radiation of short duration and fast frequency drift (type III emission). CME-associated shocks produce narrow-band, slow-drift electromagnetic radiation, known as type II emission, while electrons trapped in magnetic loops produce broad-band emission (type IV emission). The frequency of these emissions is associated to the plasma frequency, hence the local density, and this gives an estimate of where the emission is produced; we can thus follow their evolution from the low corona (at metric wavelengths) till the Earth (at kilometric wavelengths). Therefore, solar observations at metric wavelengths are essential both for the detection of energetic phenomena and for our understanding of the physics involved.

When we observe the Sun's photosphere with common optical telescopes, it rarely appears totally calm, with no centers of activity with spots or torches. In these centers, especially when they contain many spots, there is a particularly strong release of energy, which is manifested in principle by the increase in the temperature and brightness of the area, but can also cause the explosive appearance of a flare. Regardless of the appearance of a flare, these centers usually produce strong radio radiation characterized by an explosive increase in the energy emitted.

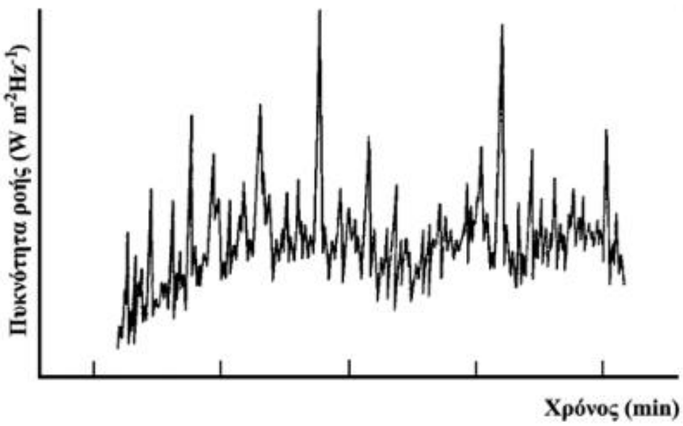

Fig. 14. Radiation Type I from the sun, using a single frequency.
[https://en.wikipedia.org/wiki/Sun]

The duration of the explosive phase ranges from a few seconds to a few hours. At low frequencies (V <500 MHz) the phenomena are very intense. First there is a strong radiation that lasts for a few seconds or minutes, and later there is a less powerful "noise" lasting for a few hours or even days. At higher frequencies (V> 500 MHz) the radiation is less intense but longer lasting from a few minutes to several hours. Because the phenomena we have just described are accompanied by rapid changes in their intensity, they are collectively referred to as a rapidly changing component of solar radiation. The simultaneous acquisition of the solar power at a number of different frequencies, generates the dynamic solar spectrum, which is usually formulated as a two-dimensional signal (image), whose horizontal axis denotes time and its vertical axis holds the frequency. Depending on the characteristics of the emitions during a radio bursts, the rapidly changing component falls into one of the following five categories.

Type I: Amplitudes of the radiation intensity in the form of noise. It is easy to see the short, narrow-bandwidth bursts. Usually occur in large numbers with underlying continuum. The duration is for every single burst ~ 1 second and the frequency range: 80 – 200 MHz. Associated Phenomena are active regions, flares, eruptive prominences. The continuous black lines are terrestrial frequencies, such as TV station or radio stations , that need to be cleared. [62]

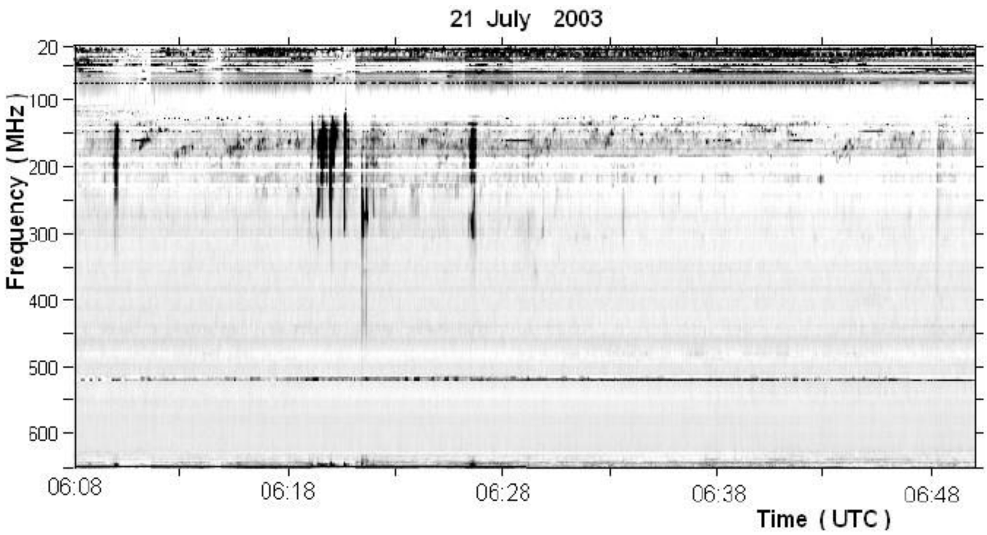

Fig.15. Typical dynamic spectrum of a Type I event.

Type II: Explosive increase of the intensity of the radiation with a slow sliding frequency (20 MHz / min). The slow frequency drift bursts is easy to be seen. Usually accompanied by a (usually stronger intensity) second harmonic. The duration is up to 3- 30 minutes and the frequency range 20 – 150 MHz. The associated phenomena are flares, proton emission and magneto-hydrodynamic shockwaves. The continuous black lines are terrestrial frequencies that need to be cleared such as t v station or radio stations. [17], [23], [38]

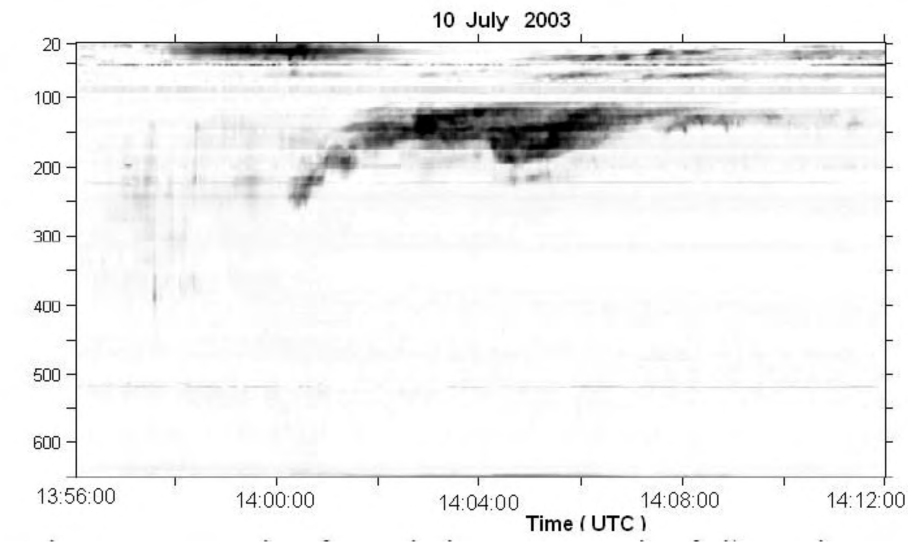

Fig.16. Typical dynamic spectrum of a Type II event.

Type III: Like type II but with rapid slip (20 MHz / s).The fast frequency drift bursts can be seen on the image and it can occur singularly, in groups, or storms (often with under lying continuum). It can be accompanied by a second harmonic with a duration for every single burst up to 1 - 3 seconds, for a group up to 1 -5 minutes and for the storm up to minutes – hours. The frequency range is 10 kHz – 1 GHz and the associated phenomena are active regions, flares. The continuous white lines are terrestrial frequencies that have been cleaned up with algorithm, such as t v station or radio stations. [4],[44]

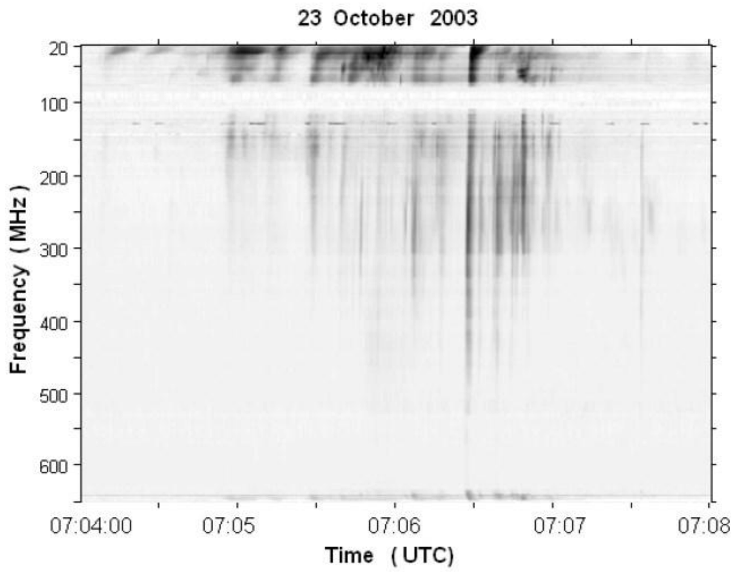

Fig.17. Typical dynamic spectrum of a Type III event.

- ***Type IV:*** Continuous long-range radiation. This radiation is observed after Type II radio bursts. It easy to observe the Stationary Type IV broadband continuum with fine structure with a duration of Hours and frequency range up to 20 MHz – 2 GHz. The associated phenomena are flares and proton emission. You can also observe a column that is seen in the figure which is the calibration time of the instrument itself. [17],[45]

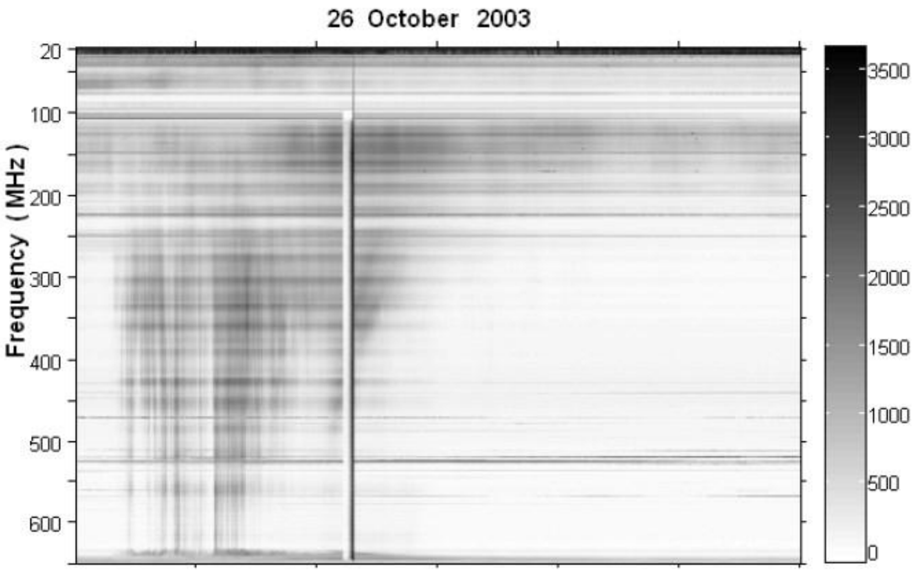

Fig.18. Typical dynamic spectrum of a Type IV event

Type V: Continuous long-range radiation, mainly at low frequencies. This radiation is observed after Type III radiation. It is a smooth, short-lived continuum burst that follows some type III bursts and never occur in isolation. The duration is up to 1-3 minutes and the frequency range 10 - 200 MHz. It is easy to see that the associated phenomena are the same as type III bursts.[63],[64]

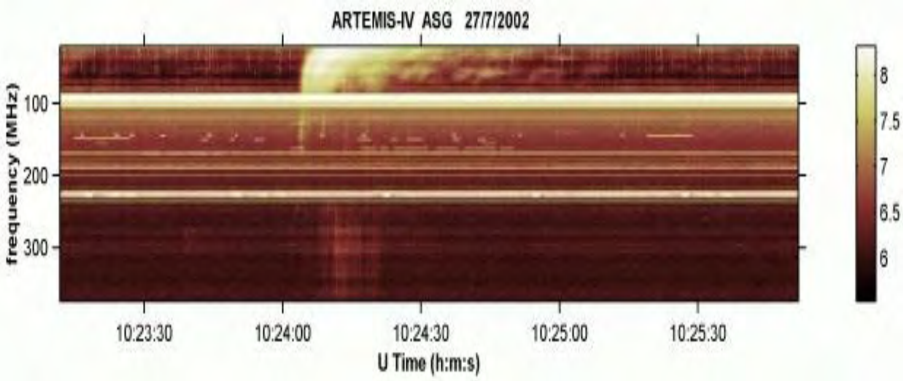

Fig.19. Typical dynamic spectrum of a Type V event

There are also some fine structures that have been observed during solar burst that have to be mentioned and analyzed such as U type herringbone like figures as shown below Fig.20. that are particularly interesting and will be studied in the future.

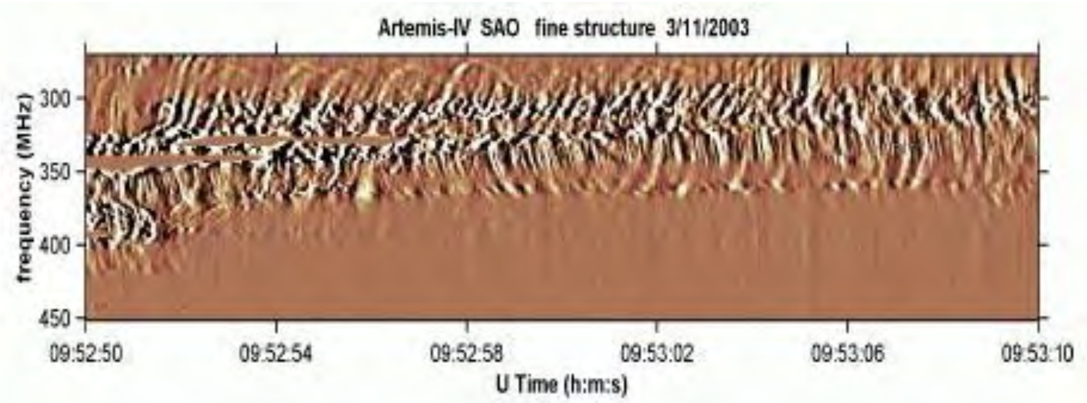

Fig.20. U type herringbone, as it appears in the solar dynamic spectrum.

Depending on their time of occurrence, the different types of radiation are classified in two phases. The first phase is Type III and V radiation. In the second phase the Type II and IV radiation. Radiation that cannot be included in the above two phases is usually characterized as Type I (Figure 3.6). Type I radiation occurs usually sporadically, a few minutes after the eruption of a solar flare, and usually takes only a few seconds or minutes. It is believed to be due to rapidly moving particles produced during flare. [41],[42],[43].

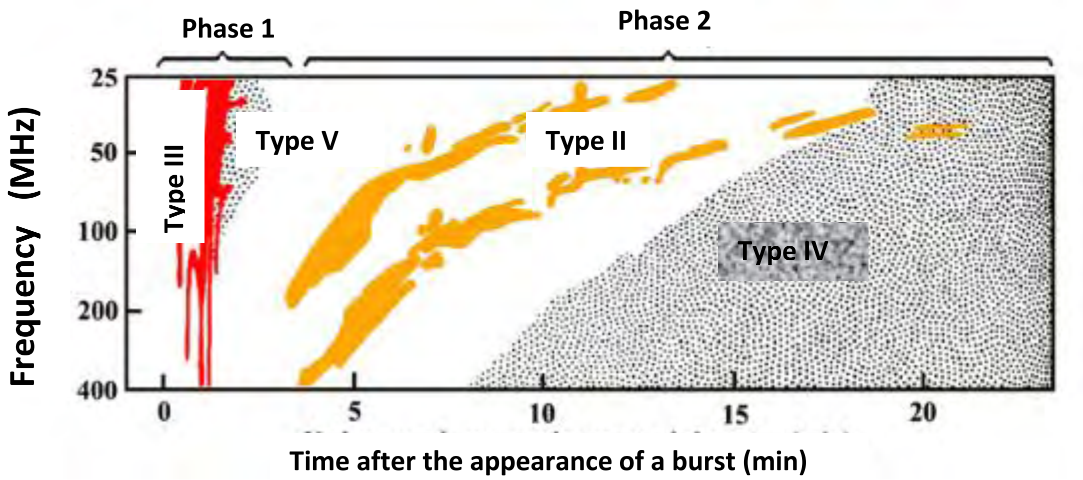

Fig.21. Brief diagram of the different types of solar radiation on radio waves.

The main feature of the first phase is the sudden, intense and short-term increase in radiation, usually after an outbreak occurs. The increase in radiation is first observed at relatively high frequencies (~ 500 MHz). Its range is very narrow, 1 - 2 MHz, and within a few seconds "slides" to smaller frequencies up to 20 - 25 MHz. Observation of the slip is achieved by special amplifiers, which cover a wide range of frequencies. Figure 15 illustrates the image we get from such an amplifier.

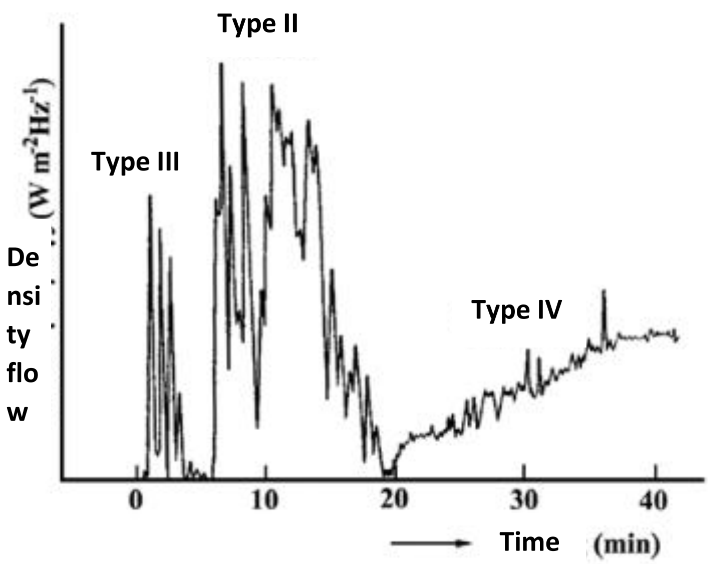

Fig.22. Records of solar activity on radio wavelengths.

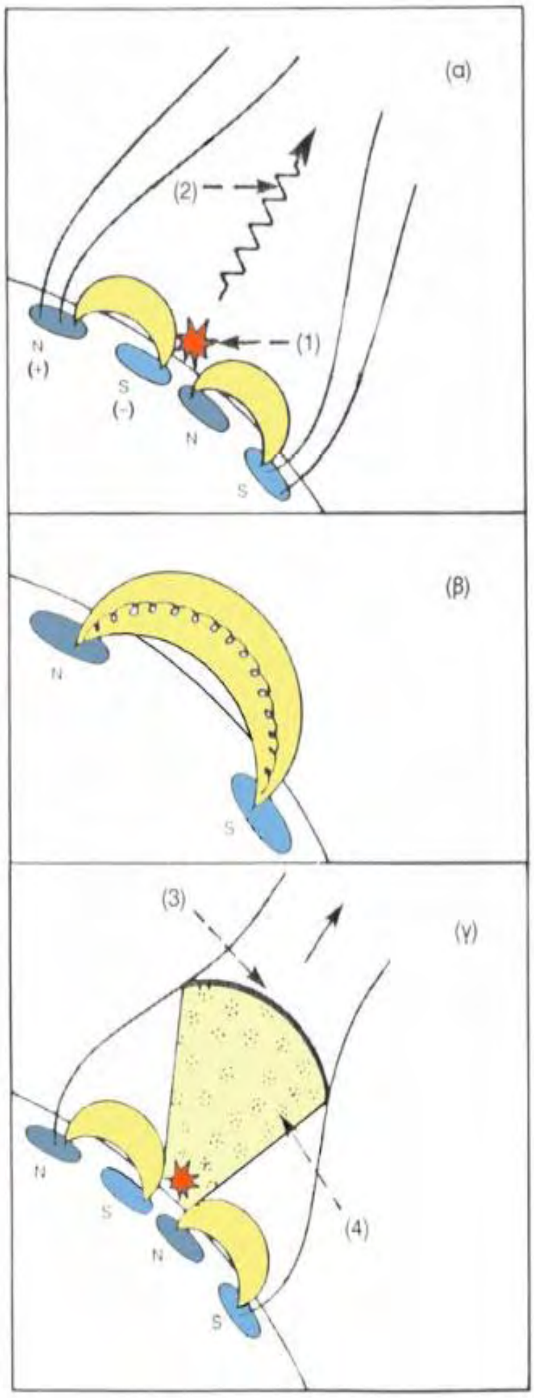

(a) Reconnecting the magnetic dynamic lines to the area of a set of spots causes the initial release of energy (flicker) (1). Charged particles (mainly electrons) are accelerated by the explosion and at high speed are removed from the area causing plasma vibrations and emission of Type III radio waves (2).

(b) High energy electrons are trapped by the strong field of the area and rapidly moving on helical paths between the poles of the Type V).

(c) The impacted wave front is removed from the point of explosion at a speed of about 1000 km / s causing plasma vibrations and Type II radiation (3). The electrons within the magnetic field located behind the shock wave front emit synchrotron radiation, Type IV (4).

Fig.23. Production of different types of radio radiation during flares.

If observations are made with narrowband frequency amplifiers, then the intensity of the radiation from the Sun after a strong flare is given in Fig. 18. Although in such recordings we cannot observe the sliding frequency, we can easily discern the various types of broadcast mentioned above.

Type III radiation is characterized by a rapid sliding of the radiation intensity (~ 20 MHz/s) from large frequencies to smaller ones. This radiation occurs immediately after the onset of a flare. If the flare is strong, then in the first phase the Type V emission occurs, mainly at low frequencies. Type III emission is due to a rapidly moving electron beam (~100000 km/s) from the area of flare accompanied by plasma vibrations . The movement of the beam to the upper layers of the Sun's atmosphere is confirmed by the observed frequency slip. The frequency of plasma oscillations depends on the number of electrons, which decreases as the beam is removed from the Sun's surface. Particles of charged particles of solar origin have been observed even in the Earth's neighborhood where the frequency of plasma vibrations has dropped to approximately 20 kHz (λ = 15 km).

Type V emission is believed to be due to fast-moving electrons moving within the strong magnetic field in the area of flare. This is synchrotron radiation, which produces radio waves over a wide range of frequencies. If the initial oscillation is small, then the phenomena that accompany it at the radio wavelengths are limited to those of the first phase. But if there is a strong flare (of 3 or more) then, usually, a few minutes later, even more spectacular phenomena last longer. These phenomena (Type II and IV emissions) constitute the second phase of the rapidly changing component. The second phase begins with the emission of strong Type II radiation at high frequencies. Radiation emission is simultaneously observed over a wide range of frequencies (20-100 MHz) and its maximum is slipped at 20 MHz / min to the lower frequencies. This slip is much slower than the sliding observed during Type III radiation. As a rule, Type II radiation is accompanied by its first harmonic, which is observed simultaneously with suitable amplifiers (Figure 3.7). And in this case the emission is due to plasma vibrations from the front of a rapidly rising shock wave from the flashing area. The velocity of the shock wave is calculated at around 1000 km / s.

Sometimes the Type II broadcast is accompanied by a long-lasting "noise" of continuous radiation, which can take several hours or even days. This radiation is classified as a Type IV emission and is due to a synchrotron emission from the expanding gas that created the shock wave referred to in the previous paragraph. Indeed, high-resolution observations have shown that the source of Type IV radiation moves away from the Sun's disk at a speed of 1,000-1,500 km / s and can reach a distance of some sun rays until it falls "falling" below the sensitivity thresholds of radio telescopes.

Figure 24 illustrates the mechanism of creating the various types of the rapidly changing component of the radiating radiation from the Sun.[12],[14].

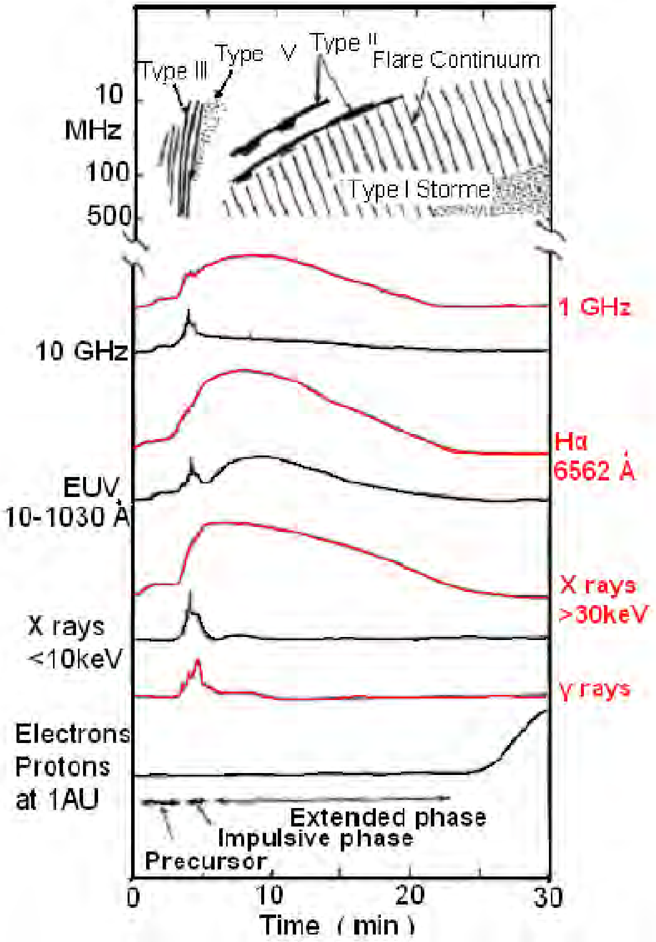

Fig.24. Representation of different phases of a typical solar burst in the electromagnetic spectrum including the practical's emission (Kane 1974). [5]

[https://en.wikipedia.org/wiki/Sun]

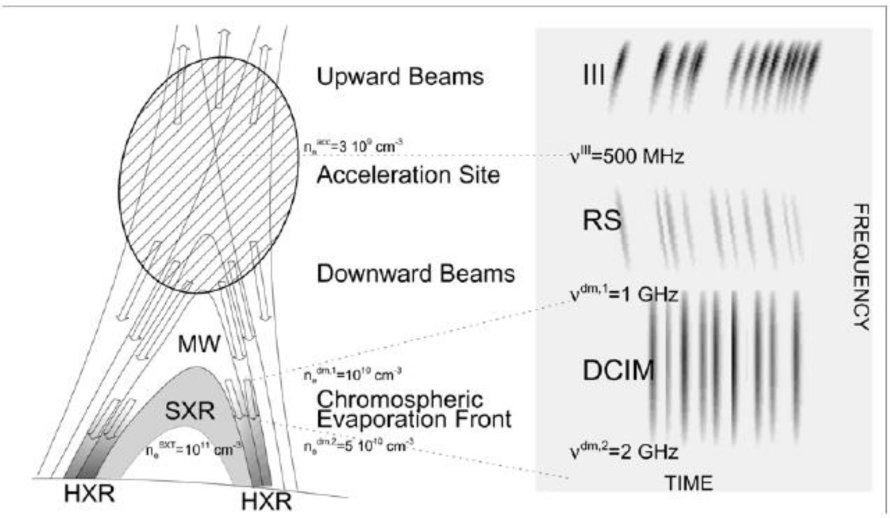

Fig.25. *[https://en.wikipedia.org/wiki/Sun]*

1.3. Instrumentation for measuring solar radio spectrum

The **ARTEMIS-IV radio spectrograph** (currently the Jean-Louis Steinberg radio spectrograph) is located in the premises of the ground-satellite station of the Greek Telecommunications Organization (OTE) at Skarfia, near Thermopylae. It was developed as a Franco-Hellenic collaboration, led by Prof. C. Caroubalos (University of Athens) and Dr J-L Bougeret (DESPA, Observatoire de Paris-Meudon) and is now operated by the University of Athens, the Technological Education Institute of Sterea Hellas in Lamia and the University of Ioannina, Greece. Its operation started in 1998; in 2017 it was renamed in the memory of the pioneer French solar radio astronomer Jean-Louis Steinberg (1922-2017).

Fig.26. The Artemis-IV Team at Thermopiles, Greece

In its present configuration, ARTEMIS-IV/JLS consists of two antennas:

- a 7m parabolic antenna with a log periodic feed for the decimetric-metric range and
- an inverted V dipole antenna for the low decametric range.

Two receivers are used: a sweep frequency receiver (ASG), with a time resolution of 100 ms and a frequency resolution of 1 MHz, fed by both antennas and covering the entire metric-decametric band from 650 to 20 MHz with a dynamic range of 70 dB, and a low noise acoustic- optic receiver (SAO), with a high time resolution (10 ms) and a frequency resolution of 1.7 MHz, fed by the metric antenna and covering the band of 450 to 270 MHz with a dynamic range of 25 db. The upper limit of the observable frequency range is set by the parabolic antenna properties and the lower limit by the ionospheric cut-off. [22],[24],[27]

1.4. Image analysis of dynamic spectrum of radio bursts.

There is a notable number of scientific papers that have image analysis proposals for the radio bursts spectrum. These papers consist of various ways in order to read data from spectrographs like Artemis IV worldwide and find new algorithms so as to process and improve the signals that are taken from the sun's atmosphere.

For example, in [46] using the Low Frequency Array (LOFAR), they have examined the spatial and temporal relation of the Type II burst to the associated CME events. The fine differences in the appearance of the dynamic spectrum between type II and IV are shown in [17]. Also different structures of type II radio bursts, like zebra patterns and spice cluster are shown in [28], [31]. In the later work, several manual measurements are performed. In [47] they performed a comparative analysis of type III solar and narrow-band type-III radio bursts properties before and during CME events in order to analyze radio observational signatures of the dynamical processes in solar corona. Furthermore in [29] simultaneous signal acquisition is performed from four different locations. In [48] they studied the disturbances come from coronal mass ejections (CMEs), and solar energetic particles (SEPs) showing that soft X-ray or microwave flux is a valuable tool to predict the CME arrival. Finally in [49] we can see from the results the possibility that flare particles could occur in all SEP events in addition to those generated by any CMEs and the association of type III-l radio bursts.

There are also many references for papers and journals that describe ways of automatic identification of radio bursts and recognition methods, in the world literature such as:

In [50] an image processing method is proposed that achieves automatic identification of type III solar radio bursts from dynamic spectral images using the Radon transform and detecting the angles that maximize an appropriate metric. Another automatic recognition proposal of coronal type II radio bursts: the automated radio burst identification system method and first observations[51] in which type II radio bursts are automatically detected after a number of preprocessing steps, using the Hough transform to detect linear structures in the dynamic spectrums.

An alternative to Hough transform and radon transform was presented in [25]. In this work direction filters are applied to 2dD Fourier transform of an image in order to calculate the energy at different orientations. Exemplar results are presented for general purpose images as well as solar dynamic spectrums. In [52] the paper presents two new methods developed to detect type III bursts automatically in the data from High Frequency Receiver (HFR) of the STEREO/WAVES radio instrument onboard the STEREO spacecraft. The first technique is applicable to the low-frequency band (HFR-1: 125 kHz to 1.975 MHz) only. In the second technique the bursts are detected in both the low-frequency band and the high-frequency band (HFR-2: 2.025 MHz to 16.025 MHz).

The automatic detection of radio bursts uses data from the Nançay Decametre Array (NDA) in the band 10 MHz–80 MHz[53]. This method eliminates unwanted signals (Radio-Frequency Interference, RFI and Calibration signals) by analyzing the dynamic spectrum of the signal recorded in time. First the calibration signals are removed and a threshold-based technique is applied to remove the background noise, using threshold values derived from the recent histogram of the dynamic spectrum. Subsequently, a gradient median filter is applied to smooth and to reduce the variability of the signal, followed by a median filter.

Finally, the events are detected using the CFAR method. Furthermore in [56] a digital signal processing technique is proposed, applying Fluctuation Analysis (DFA) to the power of te measured signal at a narrow X-ray frequency band. The selected and analyzed flares of June 06, 2000 are eruptive phenomena observed as Solar Radio Bursts (SRB) by means of the 3 GHz Ondrejov Observatory radiometer.

Moreover in [57] flux measurement is performed from dynamic microwave observations by two radio-telescopes, the VLA and Arecibo. Also image-based analysis algorithms are applied to an extragalactic signal acquired using swept-frequency techniques [58]. Flux measurements derive from the intensity of four different wavelength emission ranging from 3 to 20 cm are performed on type I c supernova, beginning 4 days after the gamma-ray burst with energy U_e associated with the radio-emitting relativistic electrons [59].

Last but not least a real-time method is presented in [61] to automatically detect and classify radio bursts in solar radio spectrographs using image gradient and mathematical morphology.

1.5. The aim of this thesis

The aim of the thesis is basically to find initially a new, easier, more reliable and efficient way to import data files from the spectrograph Artemis IV. Moreover the purpose of writing code in matlab , is to preprocess the data in image format to facilitate analysis and event detection and recognition , of solar events that are downloaded by the instrumentation of the facilities that are in our possession, meaning not only the radio spectrograph and the radio telescope Artemis IV JL Steinberg. Furthermore it is the initial work to be done with the existing data of the spectrograph in order to combine them with data received from the optical telescope “plane wave CDK 17’ ” that is situated at Hypati observatory, Fthiotida, Greece and NASA’s satellites STEREO-A, STEREO-B and WIND that already are in operation, in order to develop new methods of detecting and predicting the phenomena that take place on sun’s atmosphere. Detection of solar activity in real time is important in order to prevent dangers due to phenomena, such as radioactive solar wind and prevent failures in human activities such as airplane communication or telecommunication problems etc. Prediction of solar events is also important because it will help the evolution of space travel in our solar system in the near future and sustain life in a safer environment.

2. *Methodology*

2.1. Data acquisition by ARTEMIS IV

The acquisition system consists of two computers, one for each receiver, operating under Windows and the data are digitized with a 12-bit accuracy and stored temporarily in a hard disk, to be transferred subsequently to DVDs.

The operation of the system is automatic, and it observes the Sun from Sunrise to Sunset, recording the flux from the entire Sun as a function of frequency and time (dynamic spectrum). Quick- look daily images of dynamic spectra are available at http://artemis-iv.phys.uoa.gr/Artemis4_list.html and a catalog of type II events at http://artemis-iv.phys.uoa.gr/DataBaseForWeb/data_set_intro.htm. Interested researchers may request the original data from the ARTEMIS team.

In this configuration, ARTEMIS-IV/JLS acts both as a patrol instrument and as a high-quality research instrument, thanks to the high dynamic range of the ASG and the low noise and high time resolution of the SAO. These properties make the instrument unique worldwide.

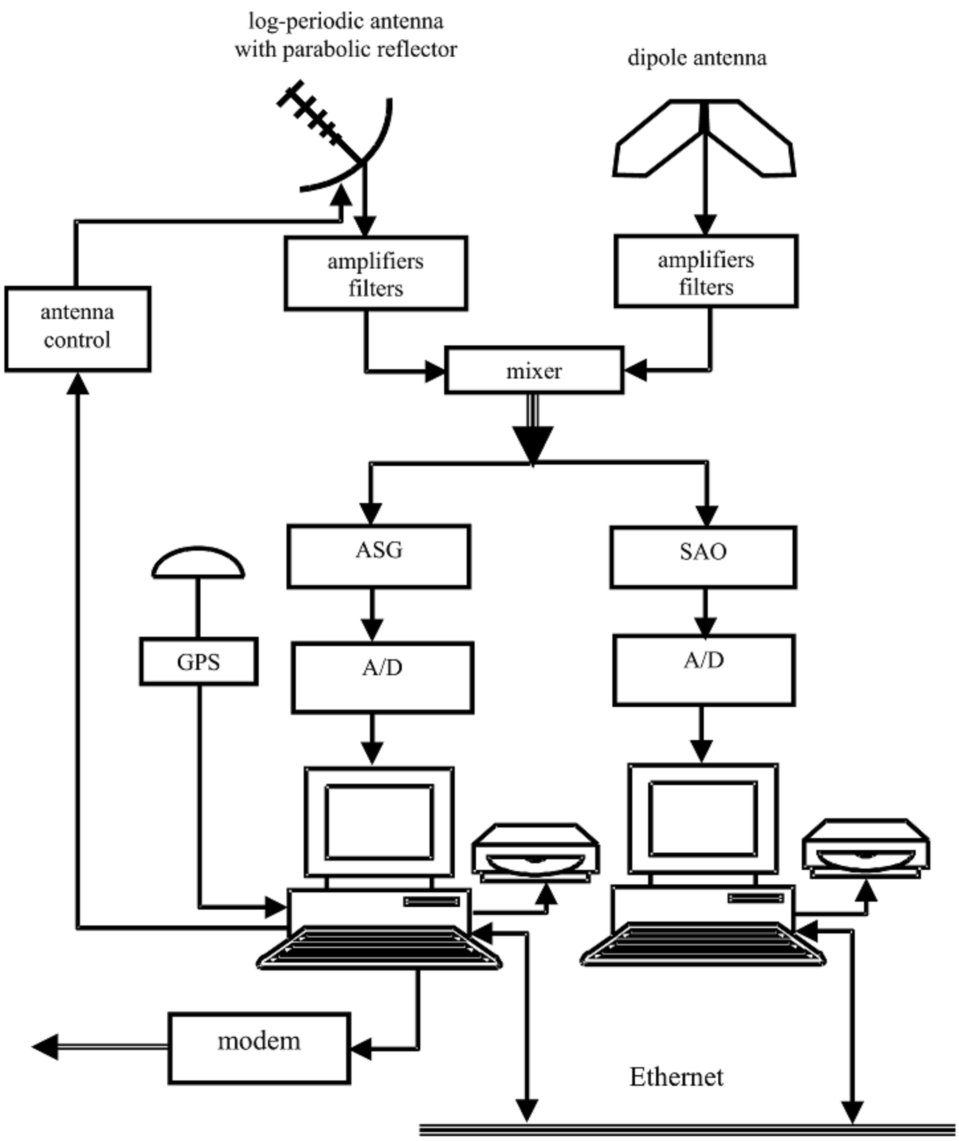

Fig.27. The Artemis IV computer-based signal acquisition system.

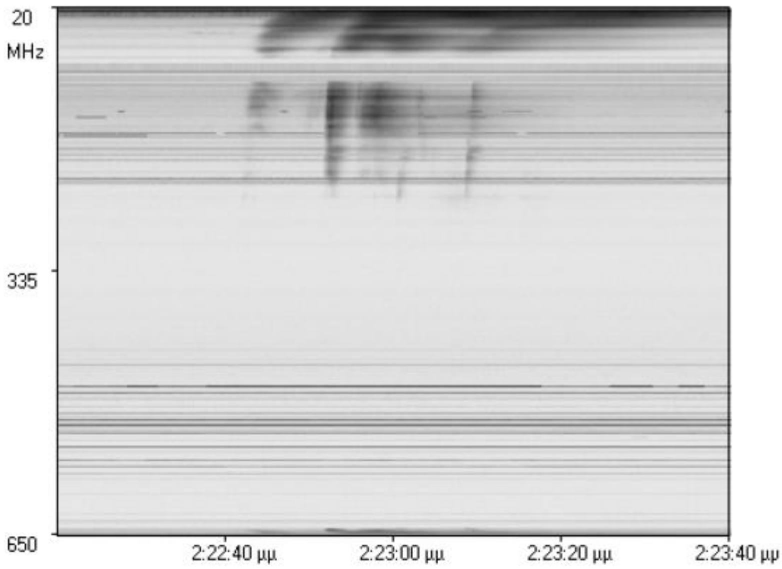

Fig. 28.

The x-axes is the UT time growing from the left to the right. The y – axes shows the frequency inverted from bottom to the top, in order to get the filing of the height that the phenomena takes place, knowing that as the emitted frequency decreases the high of the corona that the flare takes place increases.

2.2. File format

In order to store the dynamic range of the radio bursts data , that have been obtained from the Artemis IV radio spectrograph we developed a file format that allow us to restore, analyze and process the received data. Therefore the digitized measurements are been saved in a file that it consists of parts. Its part has a header followed by five continuous spectra .In the header are being stored information that make every file unique , which are considered as the ID of each file. There are also vacant posts for future use and extensions.

In particular the header has a total length of 256 bytes and consists of the following fields:

- Sequence Number Serial Number – 4 bytes
- Flags – 1 byte
- Date: described using four integer numbers with a length of 1 byte each and displayed in the following order: century, year of the century, month, day of the month. The century is obtained from the two first digits of the year the year of the century from the two last digits of it. Each of those numbers is coded in BCD binary code.

- Time: described using four integer numbers with a length of 1 byte each and displayed in the following order: hour – minutes – seconds – hundreds of seconds. Each of those numbers is coded in BCD binary code.
- 1 byte which is not used
- Number of channels: 2 bytes. This value is equal to 630 for ASG and equal to 128 for SAO files.
- Number of spectra in each part: 2 bytes. The value equals 5 and 50 for ASG and SAO files respectively
- 1 byte, which is not used
- 1 byte, which is not used
- Minimum written value inside the part – 4 bytes
- Maximum written value inside the part – 4 bytes
- Duration of spectra - 4 bytes
- Instruments code - 1 byte
- Functional method – 1 byte
- Vacant posts for future use and extensions – 122 bytes

Subsequently, 630 * 5 = 3150 integer numbers are recorded that correspond to five consecutive spectra. In each spectrum, the channels are being recorded starting from low to high frequencies. For each number, a 2 Byte storage space is required, therefor for each part the needed space is up to a total of [256 + (2*3150)] = 6556 Byte. Therefore, in order to record a 1 second signal, which consists of 10 spectra or 2 parts, 13,112 Kbyte are required. Finally for a 10 hour recording period the needed space is up to 472,032 Mbyte

2.3. Development of Software for reading ARTEMIS files

The algorithm that was implemented for reading the above file format can be described as following:

```
N=file size/(2*5*630+256)
For col=1 to N
   For I = 1 to 2
      Read 256 bytes
      B=0
      For k=1 to 5
         A←Read 630 big endian integers
         B=B+A
      end
   end
   B=B/10
   I(:,col)=B
end
```

An example of executing the file reading algorithm is shown in figure 29. The image consist of 630 lines and 2500 columns. Each column contains the value of the solar spectrum from 50 MHz to 650 MHz with a step of 1MHz.Every value is the average of ten measurements of the solar spectrum with a duration of 1ms each.

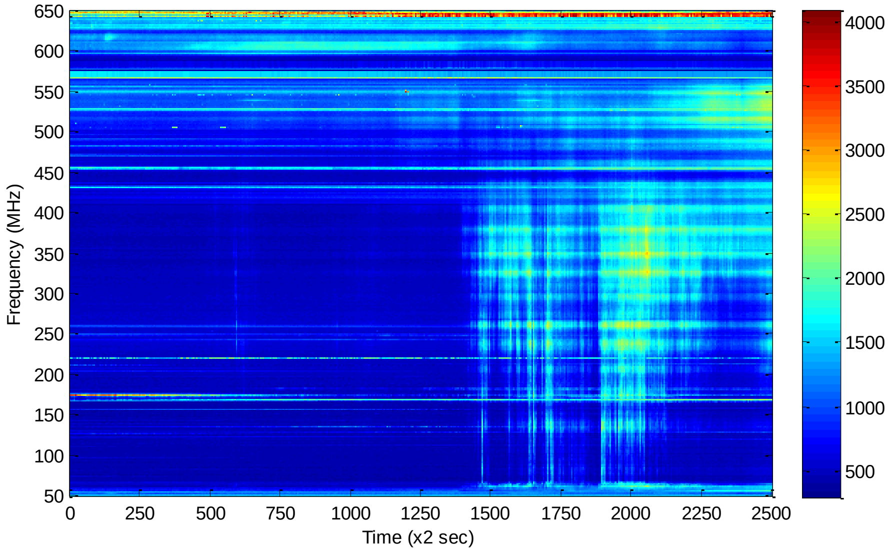

Fig. 29. The result of reading one subset of the available data.

2.4. Description of artefacts, Manual identification of events

An example of applying the file read function is shown in fig.26 for 2500 columns, each one of which is the average of ten spectrum acquired in 10ms, thus each line in the image corresponds to 100ms. The static horizontal lines in the dynamic spectrum are generated by constant radio emitions at selected frequencies, which are of terrestrial, artificial origin. The radio burst events can be seen as almost vertical in the dynamic spectrum. Manual identification of the events consists of marking the start and the end time of each event, as well as (possibly) identifying its type.

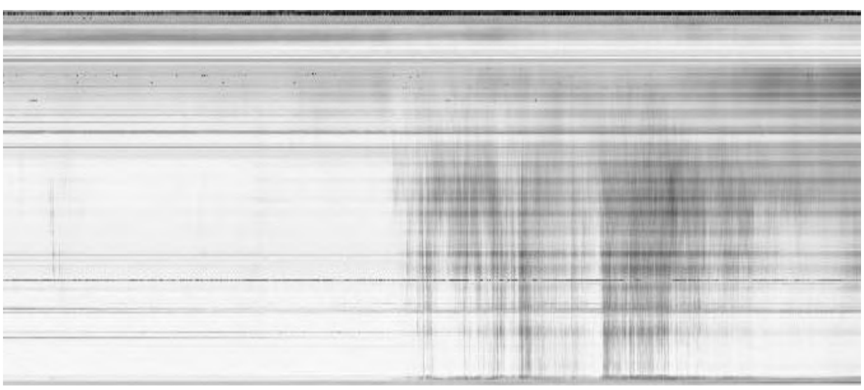

Fig.30

2.5. Image processing, Artifact removal

2.5.1. Method 1

In order to process the images that the Artemis IV has received, we apply the following method:

- We import the image, which consists of N number of lines and M number of columns, as shown below

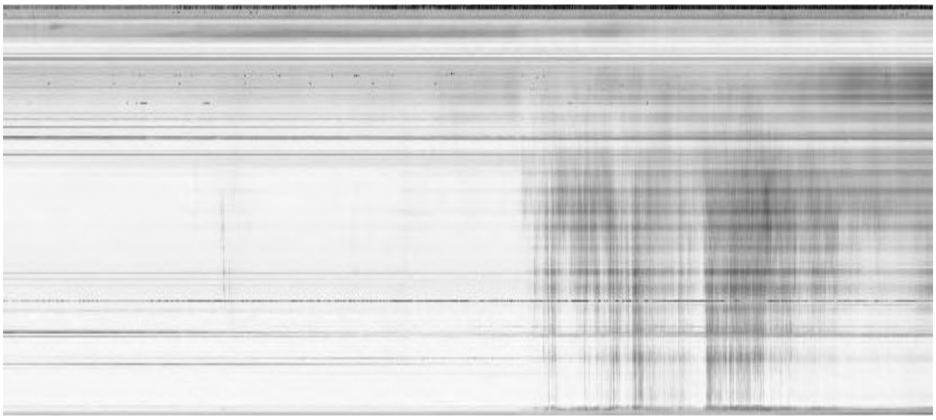

Fig.31. Initial image of type III event

- The sum of the image values is calculated along each line i, $i = 1,2,\ldots,N$:

$$s(i) = \sum_{j=1}^{M} I(i,j)$$

- Subsequently a convolution is performed using the mask:

  $mask\,(\mathrm{i}) = 1/N_m,\ i = 1,2,\ldots,N_m$.

$$\boldsymbol{p}(\boldsymbol{i}) = (\boldsymbol{s} * \boldsymbol{mask})(\boldsymbol{i})$$

As it can be verified, the sum of the elements of the mask equals 1, $\sum_{i=1}^{11} mask_i = 1$, therefore the convolution induces no gain. The result of the convolution ***p*** is a smoothed signal, shown in black color in Fig. 32, superimposed on the ***s*** signal. The positions of the continuous horizontal black lines in the image, which correspond to fixed terrestrial frequency sources, such as radio station's signals or other low frequency backgrounds from human activities are located as following: We exploit the difference of the blue curve $s(i)$ and black curve $p(i)$ to identify the line index for which the following holds:

$$s(i) \leq \boldsymbol{a}p(i)$$

where *a* is a parameter with value slightly less than 1. A typical range of values for *a* is [0.9, 0.999]. This condition identifies the image horizontal lines which represent radio emission of terrestrial origins and therefore should be removed. In this figure those lines are indicated by circles.

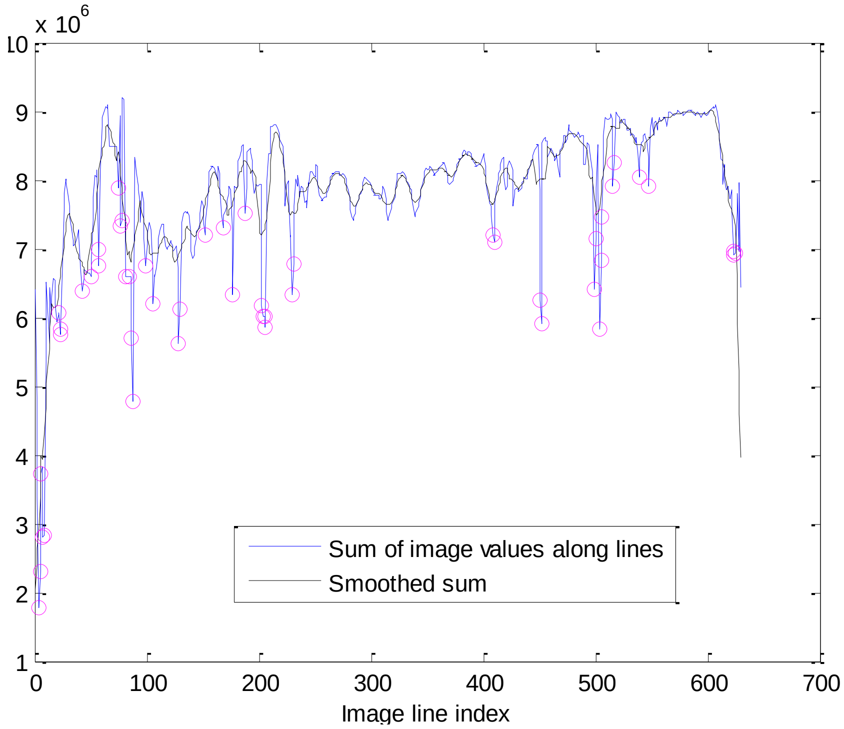

(a)

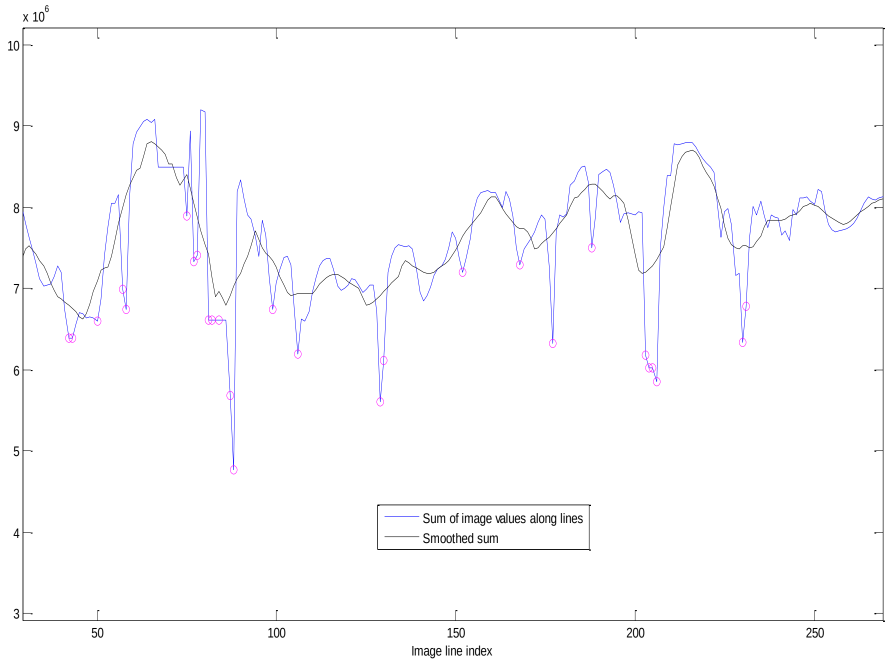

(b)

Fig.32. (a) The detected noisy horizontal lines during the 1st iteration of the proposed algorithm, with their index along the Y (frequency) axis indicated by circles, (b) a zoomed portion of the image in (a).

- After the noisy lines of terrestrial radio sources are identified, they are suppressed from the image using a vertical median filter of size $N_{med} \times 1$, applied only to the pixels of the identified lines. The concept of this filtering is shown graphically in Fig. 34.
- The above steps are repeated until no more horizontal lines are detected, or a maximum number of iterations, usually set to 20 is reached.

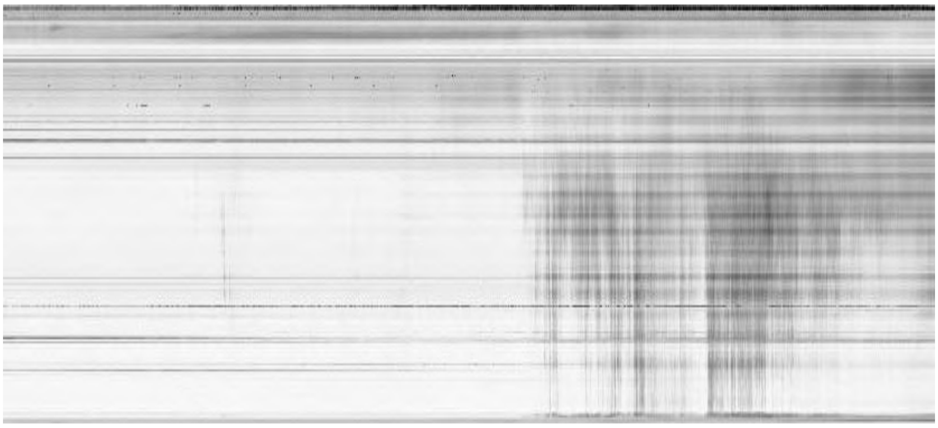

(a) initial image

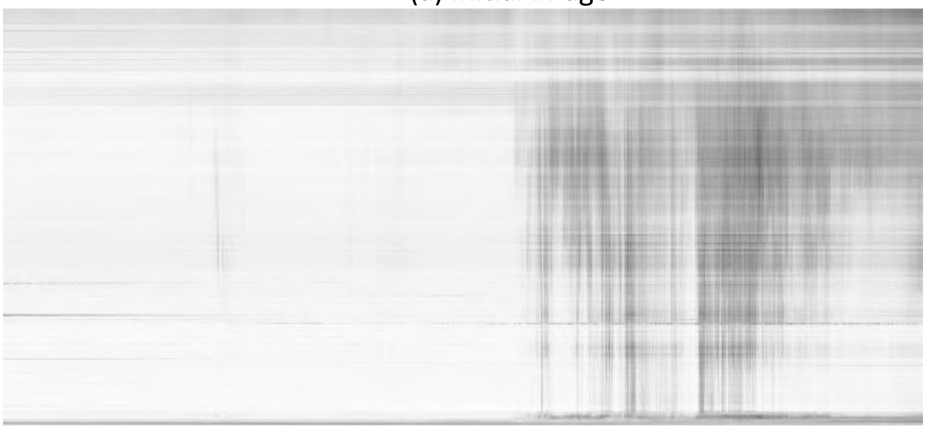

(b) the enhanced image after the first iteration of the proposed algorithm

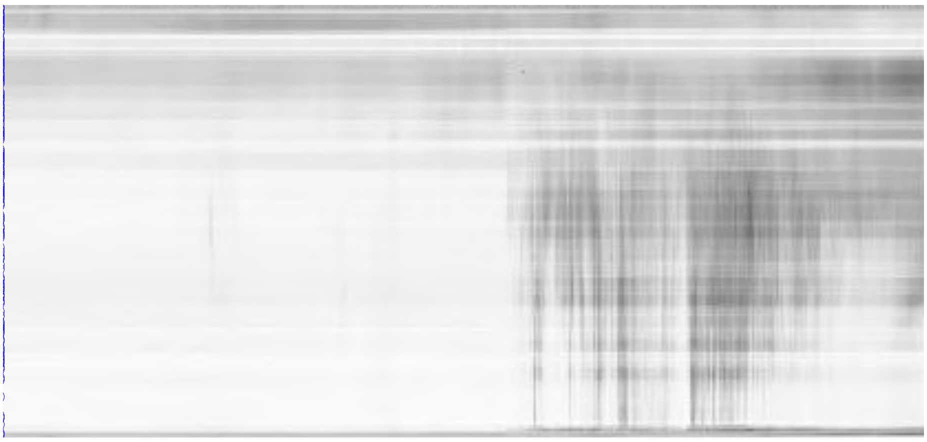

(c) enhanced image after 20 iterations

Fig.33.

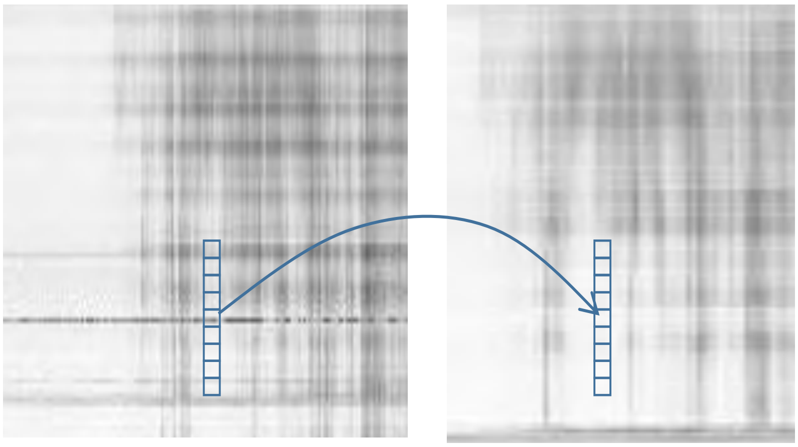

Fig.34. Schematic representation of the one dimensional vertical median filter, applied to the one of the selected horizontal lines.

2.5.2. Method 2: Fourier-based image enhancement

In this method we exploit the properties of Fourier Transform (FT) in order to enhance the visibility of the solar events of interest and suppress the rest of the image structures.

- An image that consists of N number of lines and M number of columns, was loaded as shown below.
- The DFT (Discrete Fourier Transform) was applied to the initial image.
- The logarithm of the magnitude of the transform is shown is shown in the second image of figure 35. The spatial frequency axes are super-imposed, with the zero point lying at the center of the image.
- Since the patterns of interest are vertical, we needed to keep the data of the DFT around the horizontal spatial frequency axis. Therefore, we constructed a mask with dimensions equal to the initial image by repeating the Hanning window function along all the columns of the mask, raised to the fourth power. A typical value for the width N_w of the Hanning window is 31 samples (15 samples above and below the horizontal axis). This parameter was allowed to vary, to test the results of the method. A typical image of the window function is shown in fig.36
- The mask is multiplied with the result of the DFT and the inversed DFT is applied to the product. The final result is also shown below.

We observe that the visibility of the vertical solar events is significantly enhanced and the constant terrestrial frequencies have been removed from the initial image.

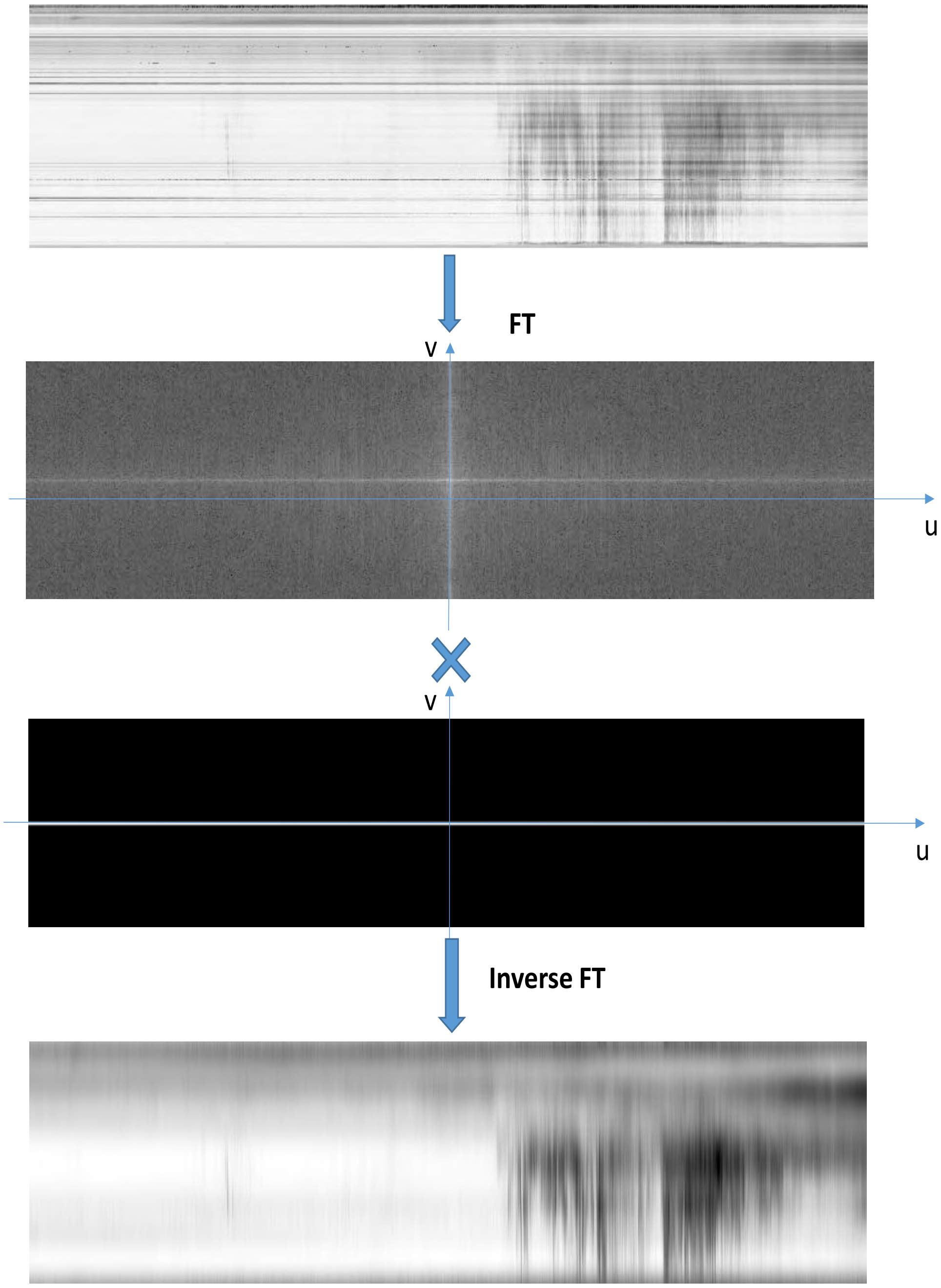

Fig.35. The intermediate steps of the 2nd (Fourier-based method).

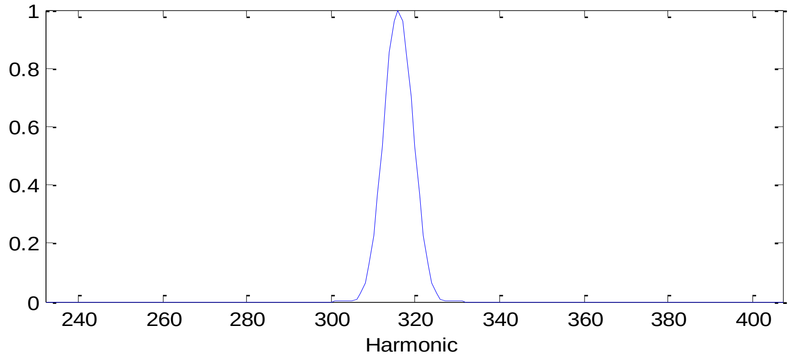

Fig.36. The window function (one dimension), used to generate the 2D window mask that was applied to the result of the DFT

3. Results

3.1. Results using method 1

In this subsection, method 1 is applied to a number of images (solar dynamic spectrums), using different values of the following parameters

- The factor a in Eq.(--) with values a=0.9 and a=0.999
- The length of the median filter N_{med} with values N_{med} =11, 41 and 71.

The initial image, as well as the resulting images are shown in the following figures for all combination of the aforementioned values of these parameters.

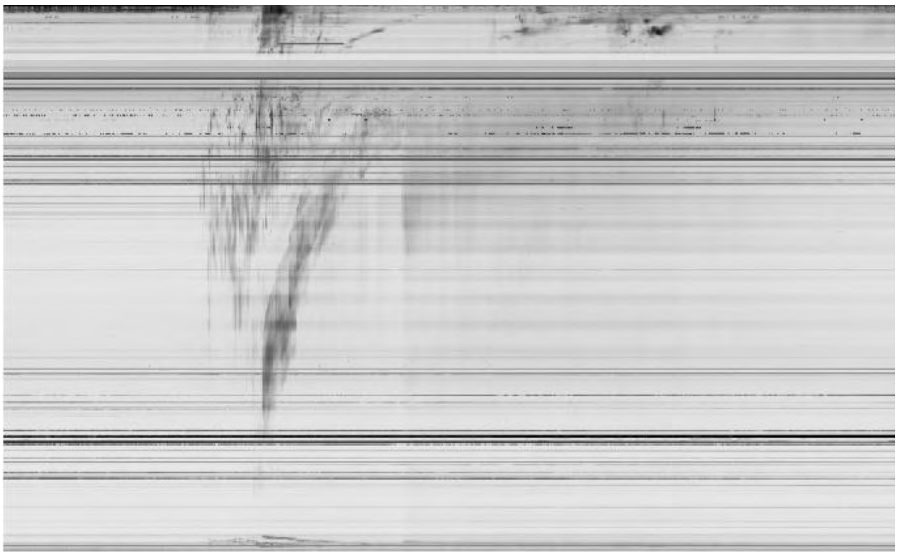

(a) initial image

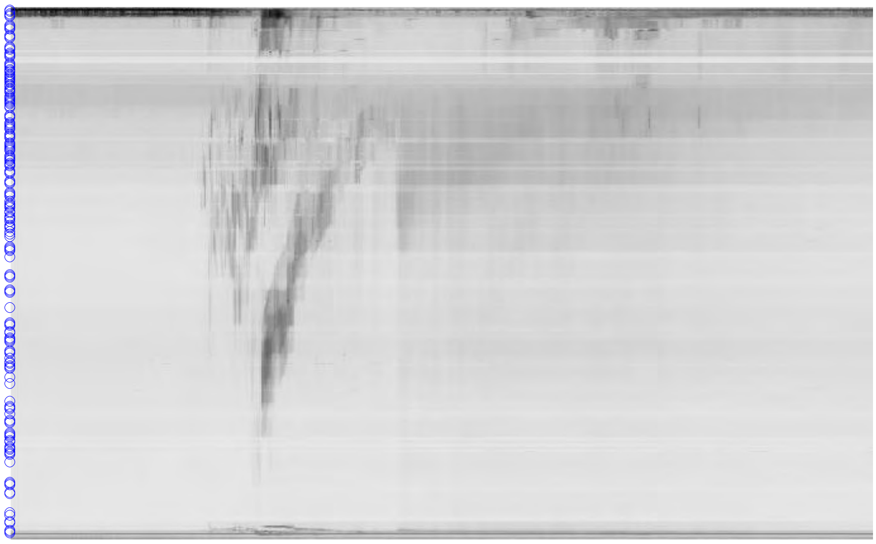
(b) The resulting image using method 1 with N_m=11, a=0.999

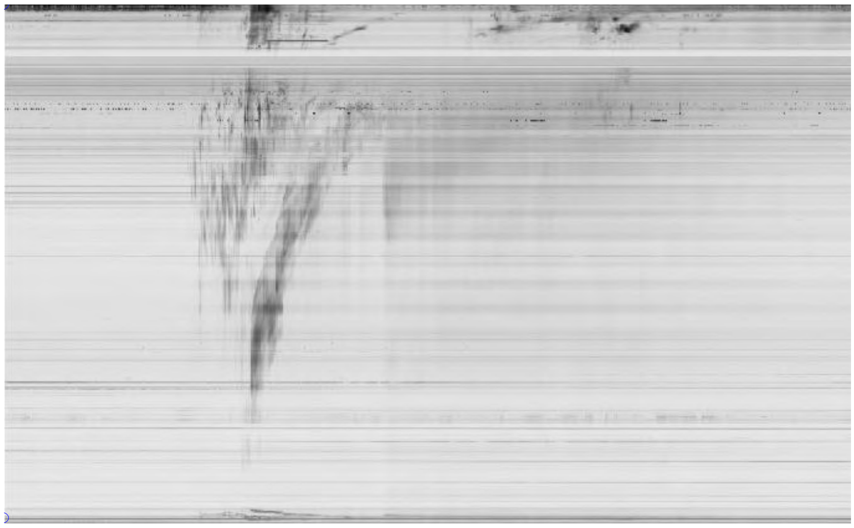
(c) The resulting image using method 1 with N_m=11, a=0.9

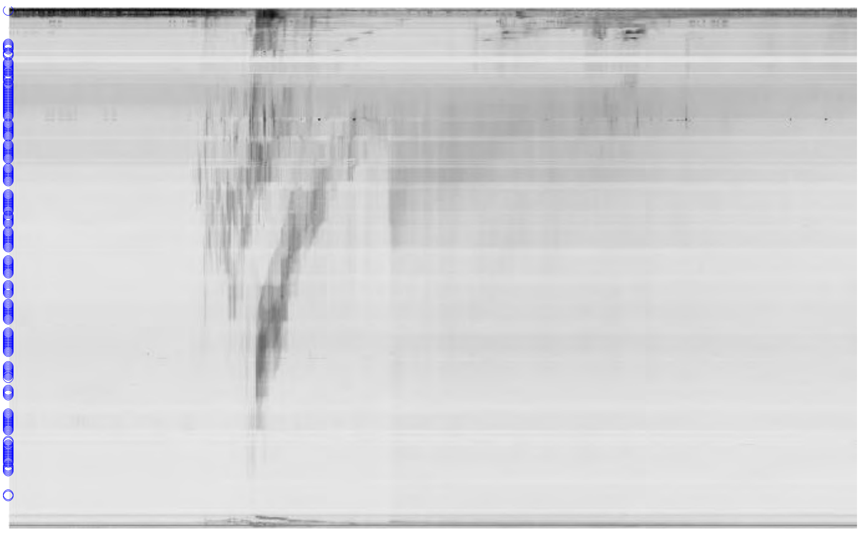
(d) The resulting image using method 1 with N_m=41, a=0.999

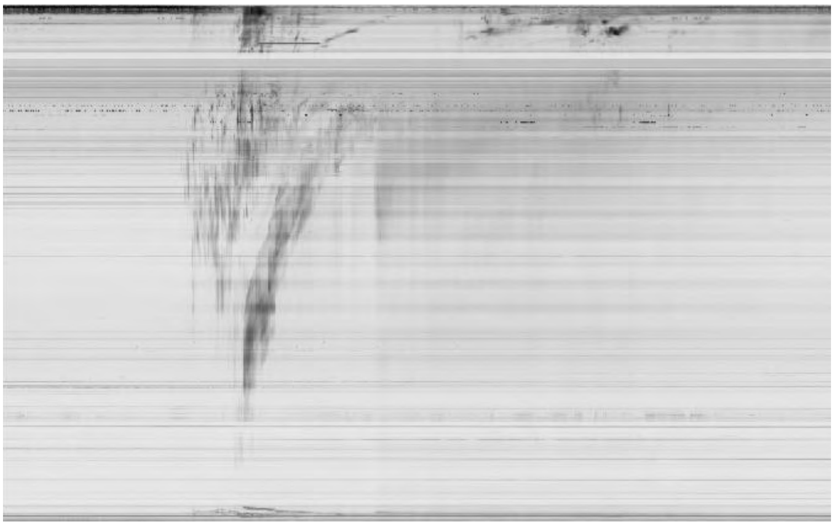

(e) The resulting image using method 1 with N_m=41, a=0.9

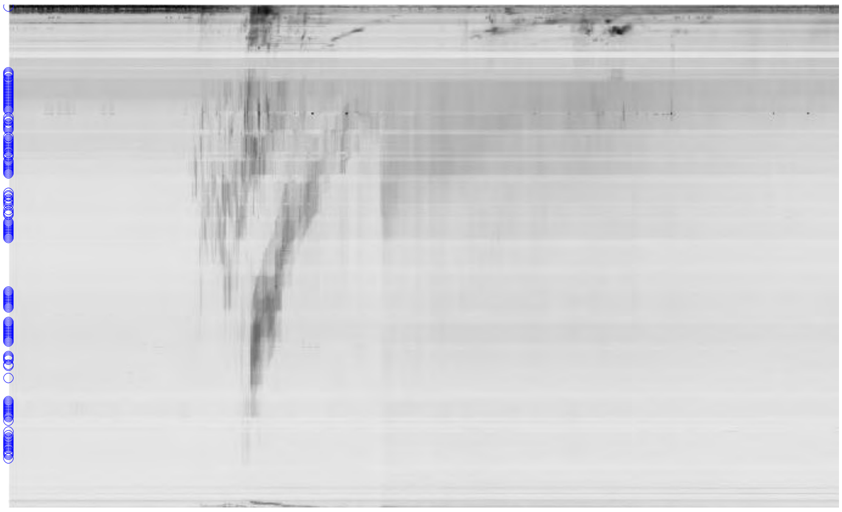

(f) The resulting image using method 1 with N_m=71, a=0.999

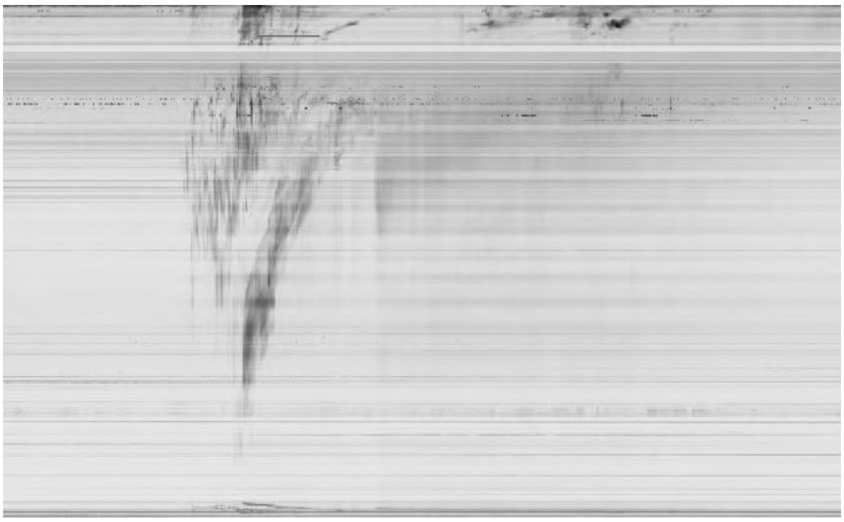

(g) The resulting image using method 1 with N_m=71, a=0.9

Fig. 3-1. Image 03B03_00 (ARTEMIS-IV ASG, 3/11/2003) containing Type II radio burst with a sliding rate of 1.82MHz / s corresponds to a shock wave moving at a speed of 2550 km/s.

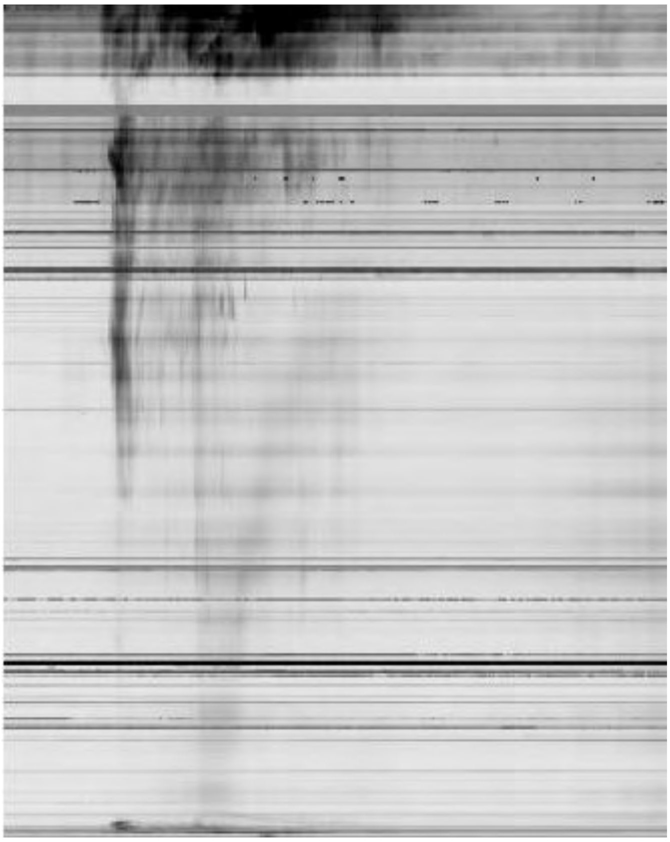

(a) initial image

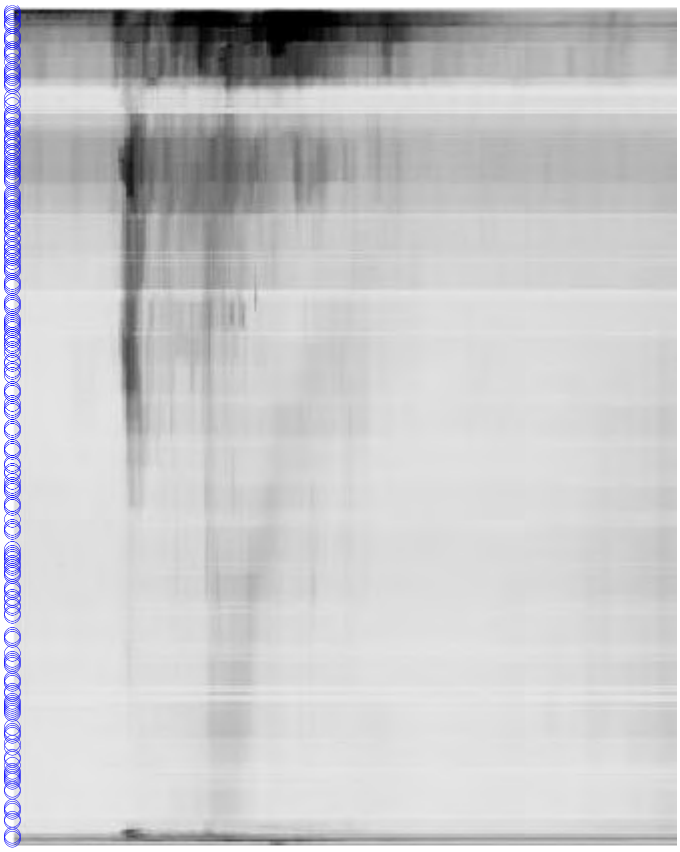

(b) The resulting image using method 1 with N_m=11, a=0.999

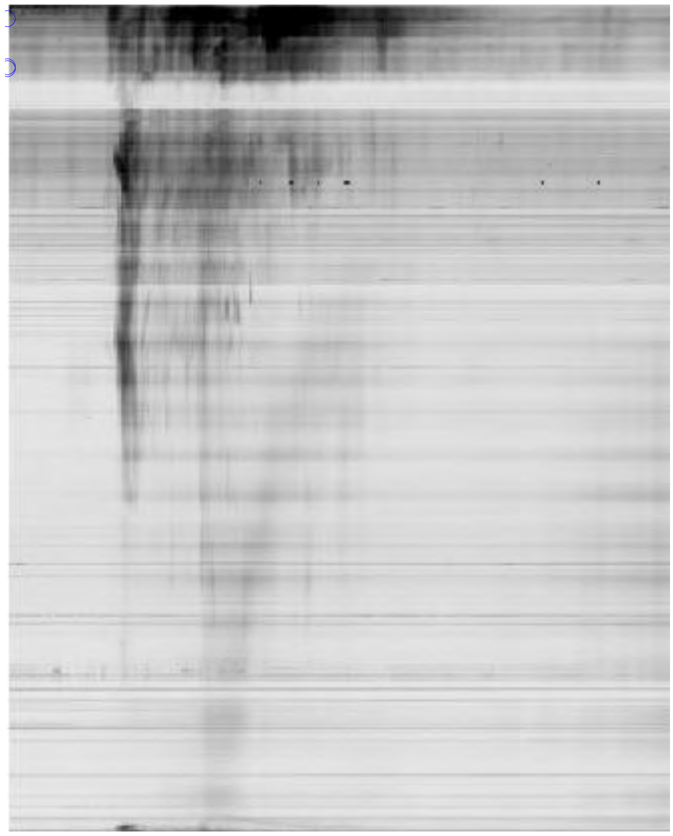

(c) The resulting image using method 1 with N_m=11, a=0.9

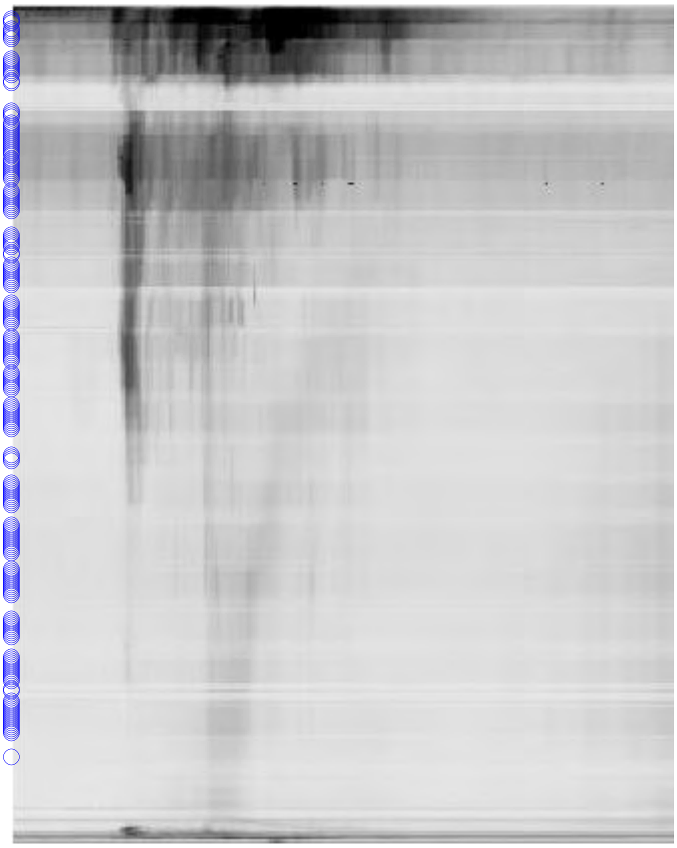

(d) The resulting image using method 1 with N_m=41, a=0.999

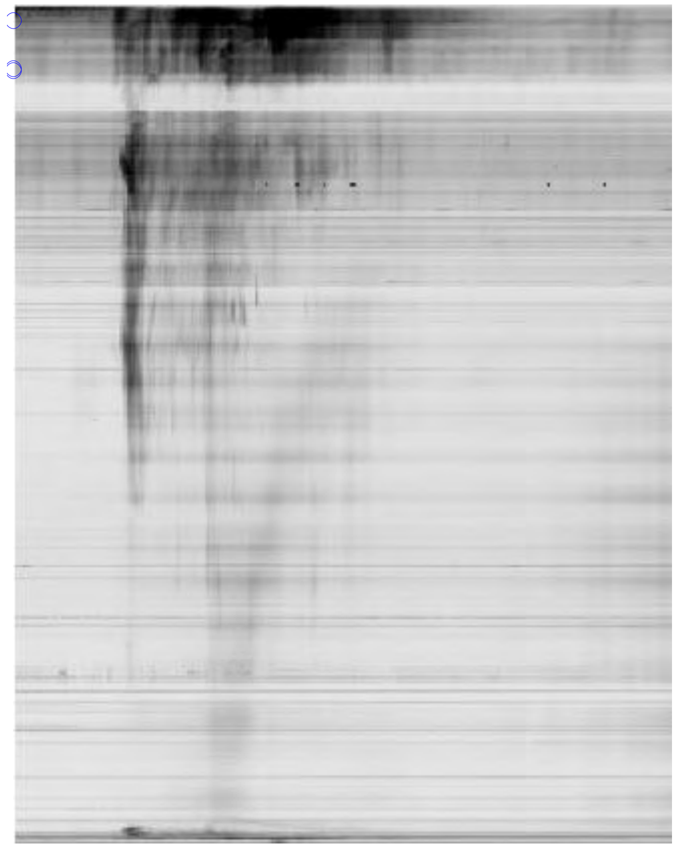

(e) The resulting image using method 1 with N_m=41, a=0.9

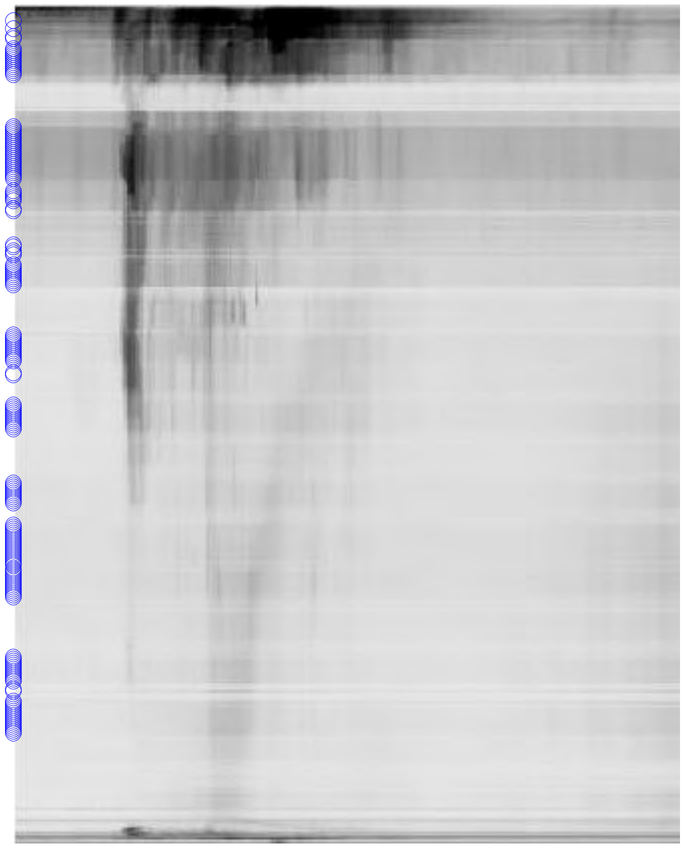

(f) The resulting image using method 1 with N_m=71, a=0.999

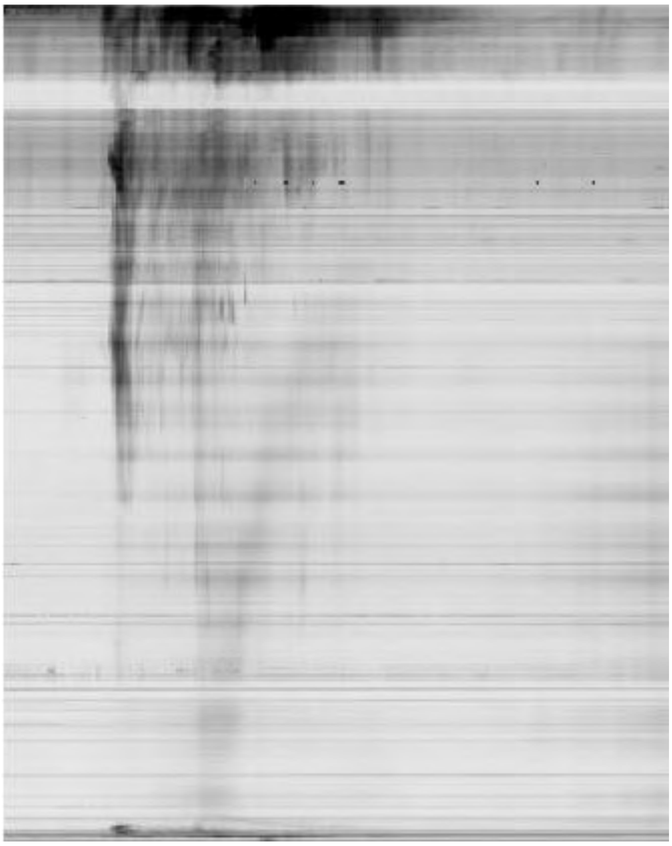

(g) The resulting image using method 1 with N_m=71, a=0.9

Fig.3-2. Image 03A28_1000 Type IV Radioburst - with intense pulse structure and sliding to lower frequencies (ARTEMIS-IV ASG , 28-10-2003) .

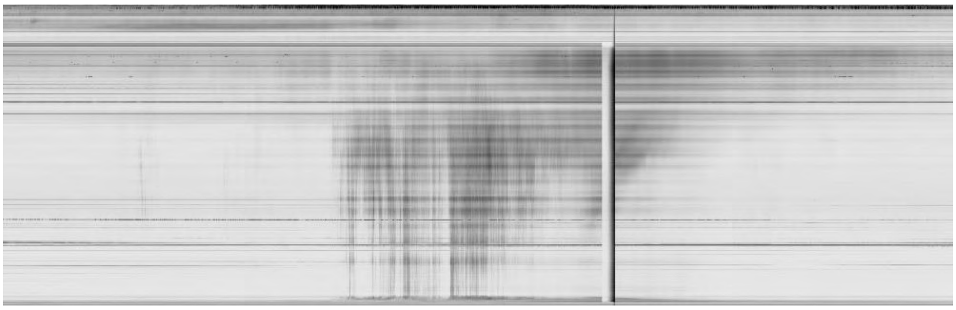

initial image

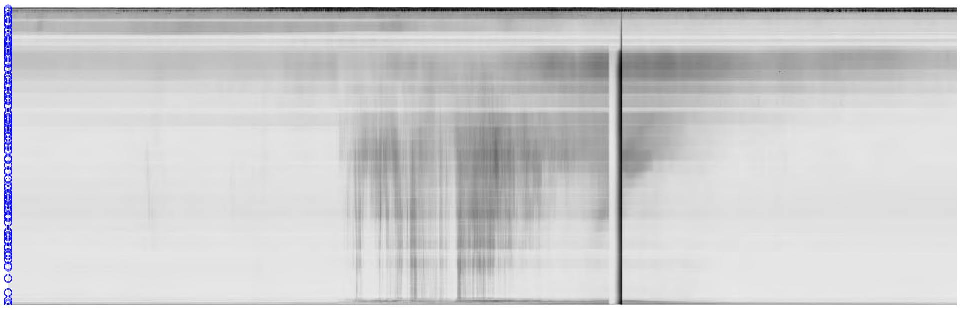

(b) The resulting image using method 1 with N_m=11, a=0.999

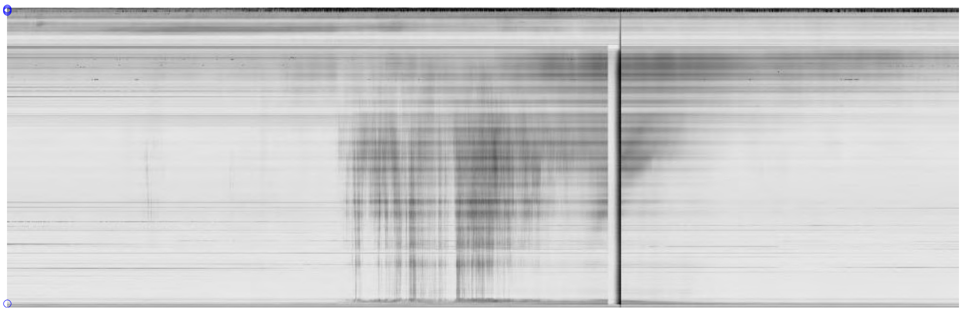

(c) The resulting image using method 1 with N_m=11, a=0.9

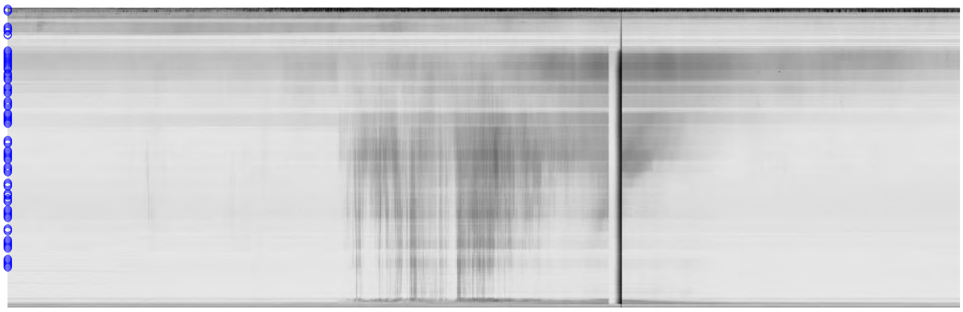

(d)The resulting image using method 1 with N_m=41, a=0.999

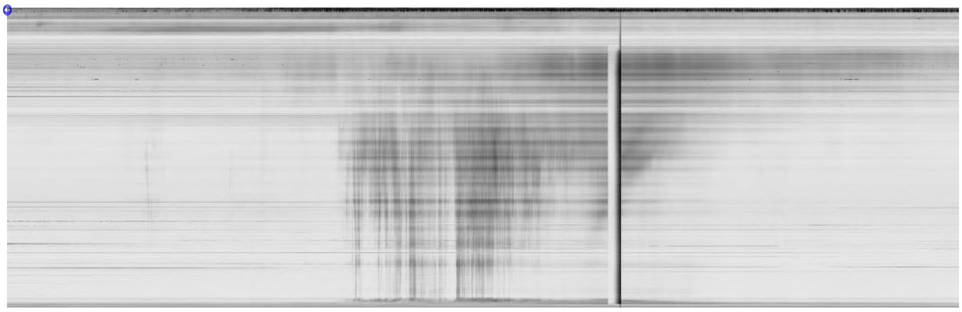

(e)The resulting image using method 1 with N_m=41, a=0.9

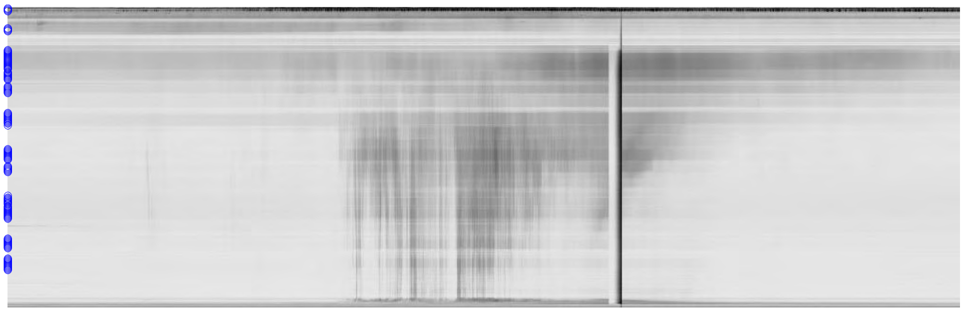

(f)The resulting image using method 1 with N_m=71, a=0.999

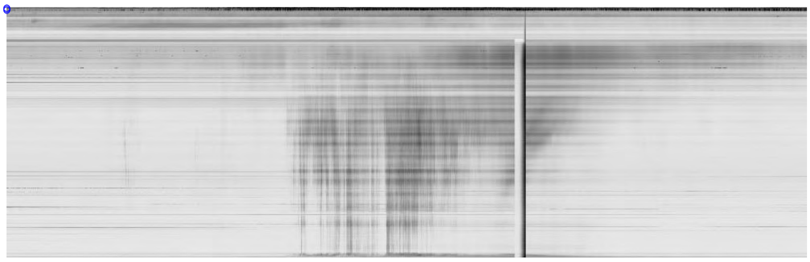

(g)The resulting image using method 1 with N_m=71, a=0.9

Fig.3-3. Image 03A26_0600 Type III -Radioburst. (narrowband spikes) (ARTEMIS-IV ASG , 26-10-2003)

3.2. Results using Method 2: Fourier-based image enhancement

This subsection shows the results of the application of the Fourier-based method to a number of dynamic solar spectrum images, containing radio bursts of different types.

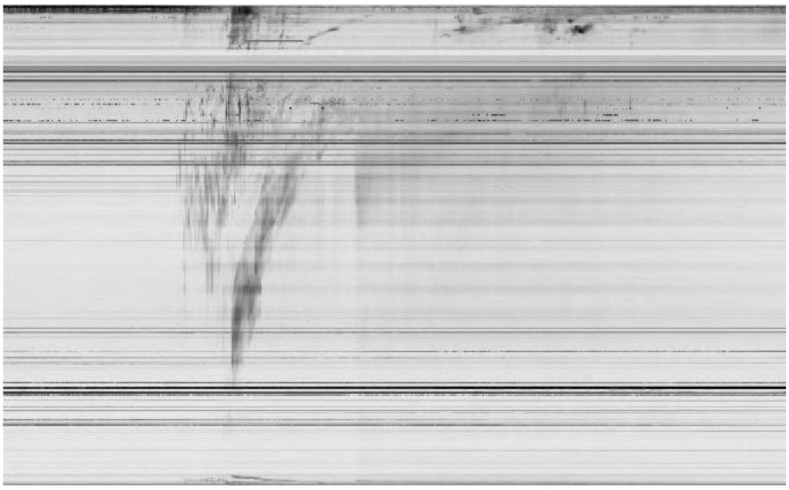

(a) initial image

(b) The resulting image using method 2 with N_w=15

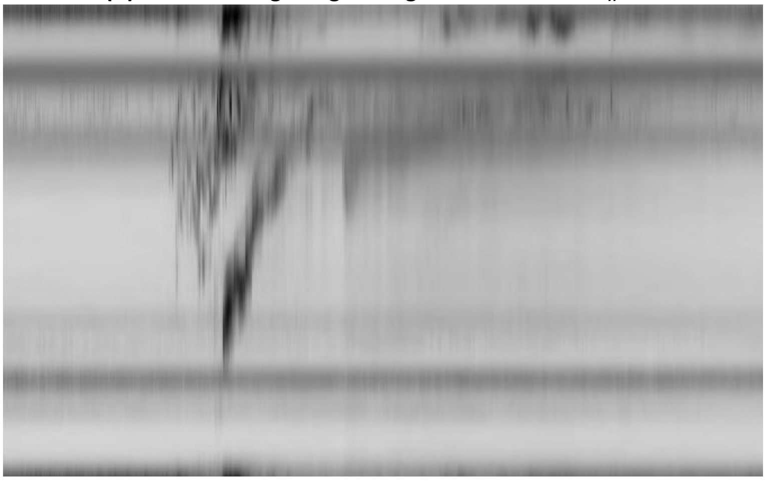

(b) The resulting image using method 2 with N_w=35

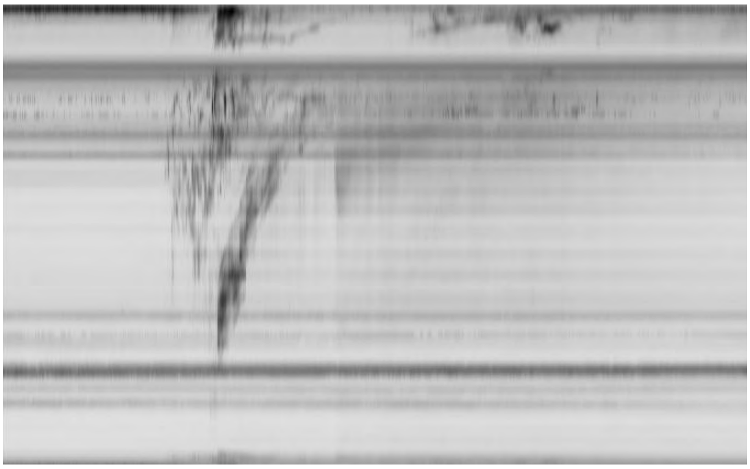

(d) The resulting image using method 2 with N_w=95

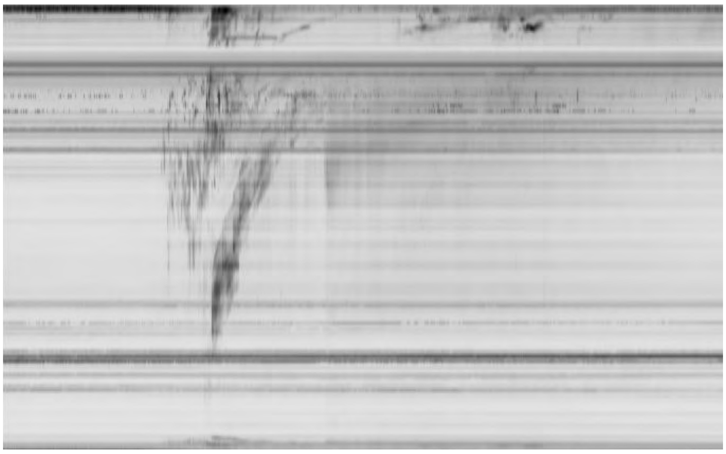

(e) The resulting image using method 2 with N_w=185

Fig. 3-1. Image 03B03_00 (ARTEMIS-IV ASG, 3/11/2003), containing Type II radio burst with a sliding rate of 1.82 MHz/s corresponds to a shock wave moving at a speed of 2550 km/s.

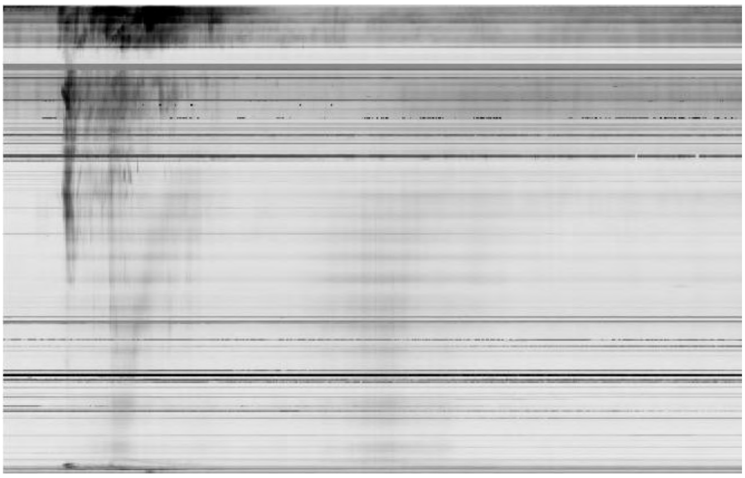

(a) initial image

(b) The resulting image using method 2 with N_w=15

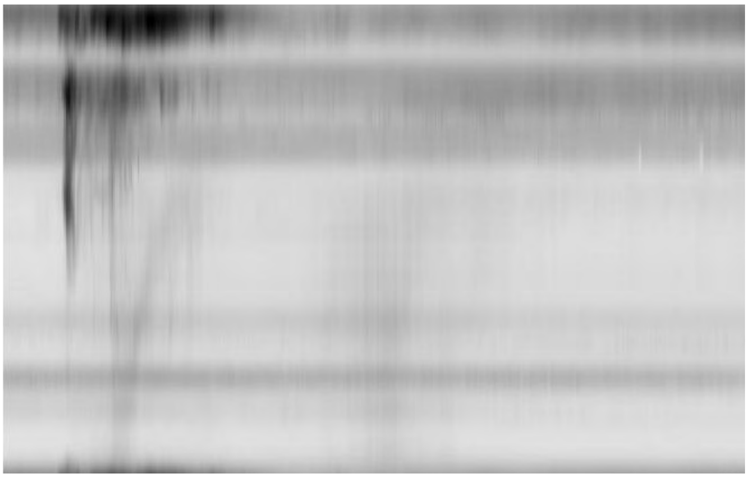

(c) The resulting image using method 2 with N_w=35

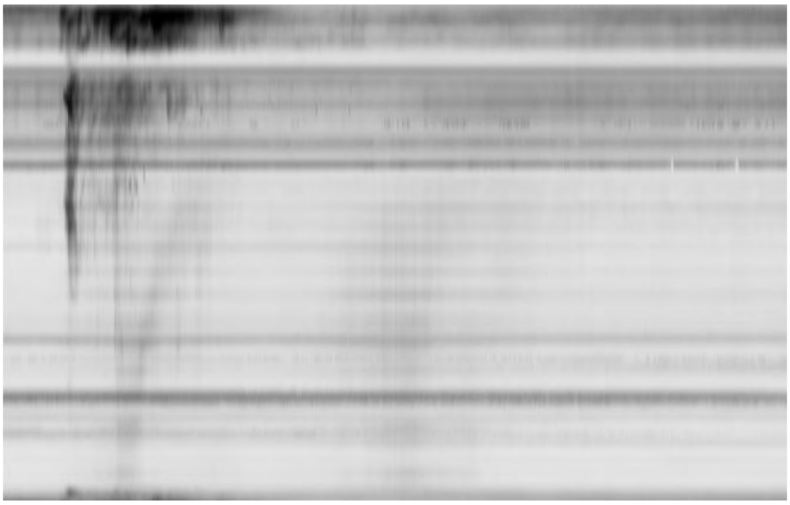

(d) The resulting image using method 2 with N_w=95

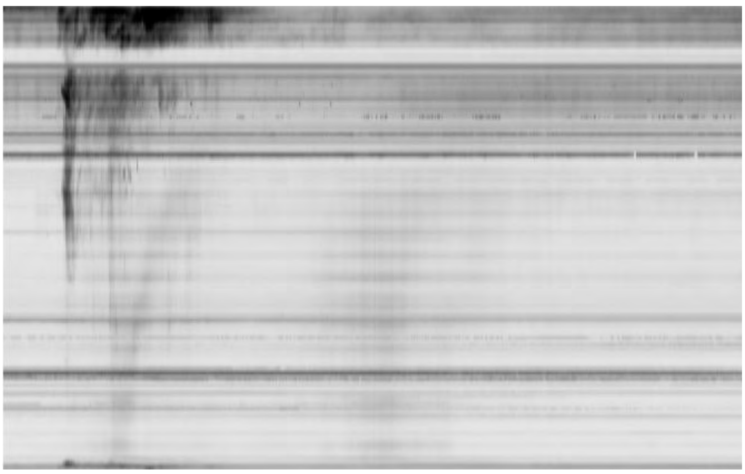

(e) The resulting image using method 2 with N_w=185

Fig.3-2. Image 03A28_1000 (ARTEMIS-IV ASG , 28-10-2003), containing Type IV Radio burst - with intense pulse structure and sliding to lower frequencies.

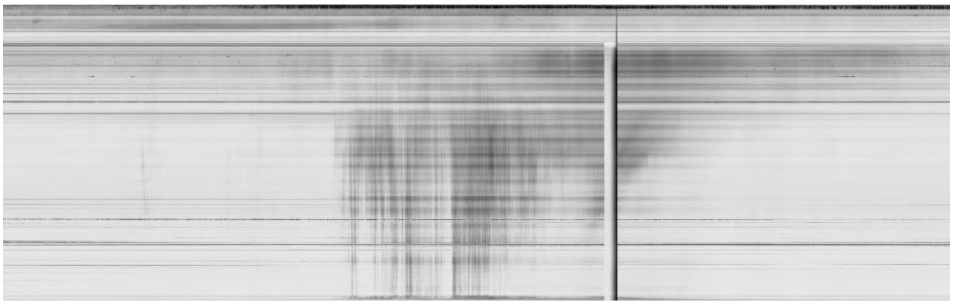

(a) initial image

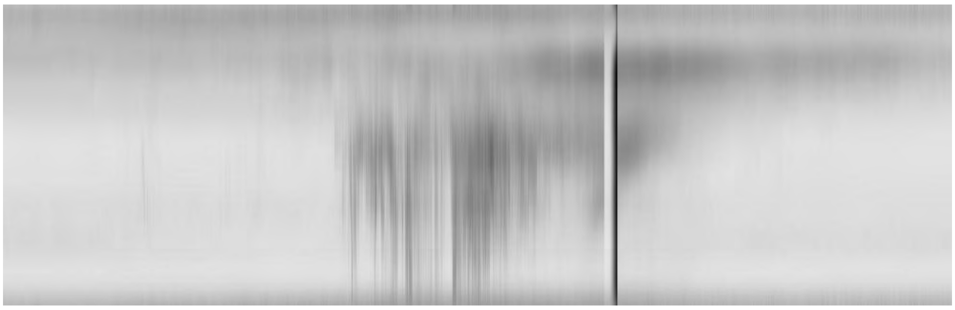

(b) The resulting image using method 2 with N_w=15

(c) The resulting image using method 2 with N_w=35

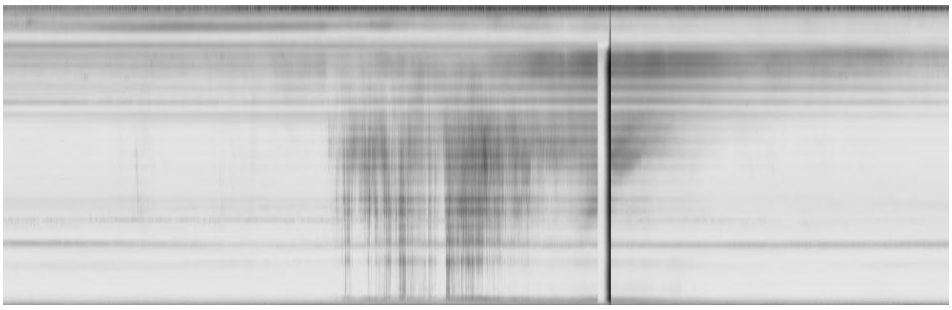

(c) The resulting image using method 2 with N_w=95

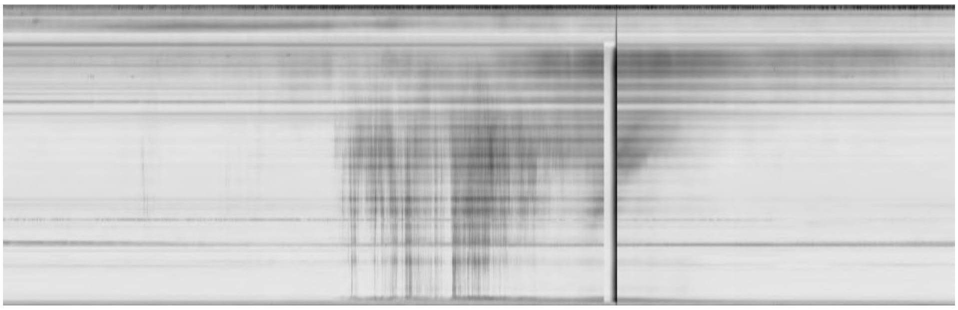

(e) The resulting image using method 2 with N_w=185

Fig.3-3. Image 03A26_0600 (ARTEMIS-IV ASG , 26-10-2003) containing Type III Radio burst (indicated by the narrowband spikes)

4. Conclusion, further work

In this work we presented the implementation of data import that are acquired from the Artemis IV spectrograph, through the years of its operation, such as observations for at list ten weak solar events associated with radio bursts (spikes) of all types. Two image processing methods were also presented and implemented, in order to pre-process the imported images and to enhance the of the radio burst patterns.

The proposed processing methods have been proven efficient in removing strong artifacts that are present in the spectrograms and are of terrestrial origin, while preserving the information about solar activity and radio bursts of all types.

The processed images may be used for further analysis, in order to automatically detect and identify the type of solar events, in real time and explore the possibility of predicting solar events.

The effect of different parameterization has also been studied in this thesis. Results were generated using method 1, with different values of the following parameters: the factor a with values 0.9 and 0.999 and the length of the median filter N med with values N_{med} =11, 41 and 71. Results show that the clearest view of the image is with values a=0.999 and N_{med} = 71.

The results using method 2 with different values of the parameter N_w = 15, 35, 95 and 185 show that the best enhancement of the event of interest was achieved using N_w = 15.

Many aspects remain to be addressed in further work.

Image analysis algorithms, including the fast emerging Deep Learning techniques can be applied for the on-line automatic detection of the radio bursts.

Combining radio electromagnetic signals and optical signals from the sun , in order to study the CME's and the radio bursts (types I,II,III,IV and V) that occur in the atmosphere of the star is a rather unexplored issue. It could provide the means to rediscover and explain the properties of radio bursts, correlate the appearance in different wavelengths and possibly help build a prognostic model. The equipment that is accessible to us consists of the optical telescope Plane Wave CDK 17 inch , Texas Instrument Corrected Dall-Kirkham on Paramount ME SOFTWARE BISQIUE Equatorial mound system with optical Sensors i) SBIG STL-11000 COOL MONO CCD SENSOR WITH FILTERWHEEL AND R-G-B,OIII,HA,SA,FILTERS and ii) ZWO ASI 1600 MC COOL COLOR CMOS SENSOR and using software i) MAXIM DL 5 and ii)THE SKY 6 PROFESSIONAL, situated at Hypati observatory Greece. This equipment can provide clear filtered images of the sun's atmosphere. The Combined observations with the two instruments can thus give both positional and high temporal and spectral resolution information of metric radio bursts.

Acknowledgement

I wish to thank Assistant Professor Kontogeorgos and Assistant Professor Tsitsipis from T.E.I. STEREAS for their help and advice throughout my thesis, as well as Professor Mousas and Assistant Professor P. Preka-Papadema from University of Athens, for providing access to data and equipment of the ARTEMIS project.

REFERENCES

1. https://en.wikipedia.org/wiki/Sun
2. https://en.wikipedia.org/wiki/Sun#Atmosphere
3. Livingston, W. C. (2002). Sun. In Allen's Astrophysical Quantities (pp. 339-380). Springer, New York, NY.
4. Alissandrakis, C. E., Nindos, A., Patsourakos, S., Kontogeorgos, A., & Tsitsipis, P. (2015). A tiny event producing an interplanetary type III burst. Astronomy & Astrophysics, 582, A52.
5. Kane, S. R. (1974). Impulsive (flash) phase of solar flares: Hard X-ray, microwave, EUV and optical observations. In Symposium-International Astronomical Union (Vol. 57, pp. 105-141). Cambridge University Press.
6. Kopp, G., Lawrence, G., & Rottman, G. (2005). The total irradiance monitor (TIM): science results. In The Solar Radiation and Climate Experiment (SORCE) (pp. 129-139). Springer, New York, NY.
7. Vemareddy, P., Ambastha, A., & Maurya, R. A. (2012). On the role of rotating sunspots in the activity of solar active region NOAA 11158. The Astrophysical Journal, 761(1), 60.
8. Christian, Eric R. (5 March 2012). "Coronal Mass Ejections". NASA/Goddard Space Flight Center. Retrieved 9 July 2013.
9. Hathaway, David H. (14 August 2014). "Coronal Mass Ejections". NASA/Marshall Space Flight Center. Retrieved 7 July 2016.
10. "Coronal Mass Ejections". NOAA/Space Weather Prediction Center. Retrieved 7 July 2016.
11. Kontogeorgos, A., Tsitsipis, P., Caroubalos, C., Moussas, X., Preka-Papadema, P., Hilaris, A., ... & Dumas, G. (2006). The improved ARTEMIS IV multichannel solar radio spectrograph of the University of Athens. Experimental Astronomy, 21(1), 41-55.
12. Bougeret SWAVES The Radio and Plasma Wave Investigation on the STEREO MissionSpaceScienceRev2008.pdf (παρ. 2.3)
13. Maroulis, D., Dumas, G., Caroubalos, C., Bougeret, J. L., Moussas, X., Alissandrakis, C., & Patavalis, N. (1997). ARTEMIS Mark-IV, THE NEW GREEK–FRENCH DIGITAL RADIO SPECTROGRAPH AT THERMOPYLES, GREECE. Solar Physics, 172(1-2), 353-360.
14. Bougeret, J. L., Zarka, P., Caroubalos, C., Karlický, M., Leblanc, Y., Maroulis, D., ... & Perche, C. (1998). A shock associated (SA) radio event and related phenomena observed from the base of the solar corona to 1 AU. Geophysical research letters, 25(14), 2513-2516.
15. Caroubalos, C., Alissandrakis, C. E., Hillaris, A., Nindos, A., Tsitsipis, P., Moussas, X., ... & Kontogeorgos, A. (2001). ARTEMIS IV radio observations of the 14 July 2000 large solar event. Solar Physics, 204(1-2), 165-177.
16. Tsitsipis, P., Kontogeorgos, A., Moussas, X., Preka-Papadema, P., Hillaris, A., Petoussis, V., ... & Dumas, G. (2006, August). Detection of slopes of linear and quasi-linear structures in noisy background, using 2D-FFT. In AIP Conference Proceedings (Vol. 848, No. 1, pp. 874-882). AIP.

17. Caroubalos, C., Hillaris, A., Bouratzis, C., Alissandrakis, C. E., Preka-Papadema, P., Polygiannakis, J., ... & Dumas, G. (2004). Solar type II and type IV radio bursts observed during 1998–2000 with the ARTEMIS-IV radiospectrograph. Astronomy & Astrophysics, 413(3), 1125-1133.
18. Pohjolainen, S., Vilmer, N., Khan, J. I., & Hillaris, A. E. (2005). Early signatures of large-scale field line opening-Multi-wavelength analysis of features connected with a "halo" CME event. Astronomy & Astrophysics, 434(1), 329-341.
19. Kuznetsov, S. N., Kurt, V. G., YU. YUSHKOV, B., Myagkova, I. N., Kudela, K., Belov, A. V., ... & Preka-Papadema, P. (2005). 28 october 2003 flare: high-energy gamma emission, type II radio emission and solar particle observations. International Journal of Modern Physics A, 20(29), 6705-6707.
20. Vršnak, B., Warmuth, A., Temmer, M., Veronig, A., Magdalenić, J., Hillaris, A., & Karlický, M. (2006). Multi-wavelength study of coronal waves associated with the CME-flare event of 3 November 2003. Astronomy & Astrophysics, 448(2), 739-752.
21. Magdalenić, J., Vršnak, B., Zlobec, P., Hillaris, A., & Messerotti, M. (2006). Classification and properties of supershort solar radio bursts. The Astrophysical Journal Letters, 642(1), L77.
22. Kontogeorgos, A., Tsitsipis, P., Moussas, X., Preka-Papadema, G., Hillaris, A., Caroubalos, C., ... & Dumas, G. (2006). Observing the Sun at 20–650 MHz at Thermopylae with Artemis. Space science reviews, 122(1-4), 169-179.
23. Hillaris, A., Petousis, V., Mitsakou, E., Vassiliou, C., Moussas, X., Polygiannakis, J., ... & Kontogeorgos, A. (2006). Solar flares with and without SOHO/LASCO coronal mass ejections and type II shocks. Advances in Space Research, 38(5), 1007-1010.
24. Kontogeorgos, A., Tsitsipis, P., Caroubalos, C., Moussas, X., Preka-Papadema, P., Hilaris, A., ... & Dumas, G. (2006). The improved ARTEMIS IV multichannel solar radio spectrograph of the University of Athens. Experimental Astronomy, 21(1), 41-55.
25. Tsitsipis, P., Kontogeorgos, A., Hillaris, A., Moussas, X., Caroubalos, C., & Preka-Papadema, P. (2007). Fast estimation of slopes of linear and quasi-linear structures in noisy background, using Fourier methods. Pattern recognition, 40(2), 563-577.
26. Lehtinen, N. J., Pohjolainen, S., Huttunen-Heikinmaa, K., Vainio, R., Valtonen, E., & Hillaris, A. E. (2008). Sources of SEP Acceleration during a Flare–CME Event. Solar Physics, 247(1), 151-169.
27. Kontogeorgos, A., Tsitsipis, P., Caroubalos, C., Moussas, X., Preka-Papadema, P., Hilaris, A., ... & Dumas, G. (2008). Measuring solar radio bursts in 20–650 MHz. Measurement, 41(3), 251-258.
28. Bouratzis, C., Preka-Papadema, P., Moussas, X., Alissandrakis, C., & Hillaris, A. (2009). Metric radio bursts and fine structures observed on 17 January, 2005. Advances in Space Research, 43(4), 605-611.
29. Caroubalos, C., Preka-Papadema, P., Mavromichalaki, H., Moussas, X., Papaioannou, A., Mitsakou, E., & Hillaris, A. (2009). Space storm measurements of the July 2005 solar extreme events from the low corona to the Earth. Advances in Space Research, 43(4), 600-604.
30. Alissandrakis, C. E., Kontogeorgos, A., Tsitsipis, P., Caroubalos, C., Moussas, X., Preka-Papadema, P., ... & Dumas, G. (2009). New Developments in ARTEMIS IV Solar Radio Spectrograph. Earth, Moon, and Planets, 104(1-4), 93-95.
31. Bouratzis, C., Preka-Papadema, P., Hillaris, A., Tsitsipis, P., Kontogeorgos, A., Kurt, V. G., & Moussas, X. (2010). Radio observations of the 20 January 2005 X-class Flare. Solar Physics, 267(2), 343-359.

32. Andriopoulou, M., Mavromichalaki, H., Preka-Papadema, P., Plainaki, C., Belov, A., & Eroshenko, E. (2011). Solar activity and the associated ground level enhancements of solar cosmic rays during solar cycle 23. Astrophysics and Space Sciences Transactions, 7(4), 439-443.

33. Nindos, A., Alissandrakis, C. E., Hillaris, A., & Preka-Papadema, P. (2011). On the relationship of shock waves to flares and coronal mass ejections. Astronomy & Astrophysics, 531, A31.

34. Hillaris, A., Malandraki, O., Klein, K. L., Preka-Papadema, P., Moussas, X., Bouratzis, C., ... & Kontogeorgos, A. (2011). The 17 January 2005 Complex Solar Radio Event Associated with Interacting Fast Coronal Mass Ejections. Solar Physics, 273(2), 493-509.

35. Malandraki, O. E., Agueda, N., Papaioannou, A., Klein, K. L., Valtonen, E., Heber, B., ... & Sanahuja, B. (2012). Scientific analysis within SEPServer–New perspectives in solar energetic particle research: The case study of the 13 July 2005 event. Solar Physics, 281(1), 333-352.

36. Miteva, R., Klein, K. L., Samwel, S. W., Nindos, A., Kouloumvakos, A., & Reid, H. (2014). Radio signatures of solar energetic particles during the 23rd solar cycle. arXiv preprint arXiv:1402.6442.

37. Vainio, R., Valtonen, E., Heber, B., Malandraki, O. E., Papaioannou, A., Klein, K. L., ... & Braune, S. (2013). The first SEPServer event catalogue~ 68-MeV solar proton events observed at 1 AU in 1996–2010. Journal of space weather and space climate, 3, A12.

38. Kouloumvakos, A., Patsourakos, S., Hillaris, A., Vourlidas, A., Preka-Papadema, P., Moussas, X., ... & Kontogeorgos, A. (2014). CME expansion as the driver of Metric Type II shock emission as revealed by self-consistent analysis of high-cadence EUV images and radio spectrograms. Solar Physics, 289(6), 2123-2139.

39. Chernov, G. P., Fomichev, V. V., Gorgutsa, R. V., Markeev, A. K., Sobolev, D. E., Hillaris, A., & Alissandrakis, K. (2014). Fine structural features of radio-frequency radiation of the solar flare of February 12, 2010. Geomagnetism and Aeronomy, 54(4), 406-415.

40. Papaioannou, A., Malandraki, O. E., Dresing, N., Heber, B., Klein, K. L., Vainio, R., ... & Mewaldt, R. A. (2014). SEPServer catalogues of solar energetic particle events at 1 AU based on STEREO recordings: 2007–2012. Astronomy & Astrophysics, 569, A96.

41. Klein, K.-L.; Masson, S.; Bouratzis, C.; Grechnev, V.; Hillaris, A.; Preka-Papadema, P.: «The relativistic solar particle event of 2005 January 20: origin of delayed particle acceleration», Astronomy & Astrophysics, 572, id.A4 (2014).

42. Bouratzis, C., Hillaris, A., Alissandrakis, C. E., Preka-Papadema, P., Moussas, X., Caroubalos, C., ... & Kontogeorgos, A. (2015). Fine structure of metric Type IV radio bursts observed with the ARTEMIS-IV radio-spectrograph: association with flares and coronal mass ejections. Solar Physics, 290(1), 219-286.

43. Kouloumvakos, A., Nindos, A., Valtonen, E., Alissandrakis, C. E., Malandraki, O., Tsitsipis, P., ... & Hillaris, A. (2015). Properties of solar energetic particle events inferred from their associated radio emission. Astronomy & Astrophysics, 580, A80.

44. Alissandrakis, C. E., Nindos, A., Patsourakos, S., Kontogeorgos, A., & Tsitsipis, P. (2015). A tiny event producing an interplanetary type III burst. Astronomy & Astrophysics, 582, A52.

45. Bouratzis, C., Hillaris, A., Alissandrakis, C. E., Preka-Papadema, P., Moussas, X., Caroubalos, C., ... & Kontogeorgos, A. (2016). High resolution observations with

Artemis-IV and the NRH-I. Type IV associated narrow-band bursts. Astronomy & Astrophysics, 586, A29.

46. Chrysaphi, N., Kontar, E. P., Holman, G. D., & Temmer, M. (2018). CME-driven Shock and Type II Solar Radio Burst Band Splitting. *The Astrophysical Journal*, *868*(2), 79.

47. Dididze, G., Shergelashvili, B. M., Melnik, V. N., Dorovskyy, V. V., Brazhenko, A. I., Poedts, S., ... & Khodachenko, M. (2019). Comparative analysis of solar radio bursts before and during CME propagation. *Astronomy & Astrophysics*, *625*, A63.

48. Klein, K. L., Matamoros, C. S., & Zucca, P. (2018). Solar radio bursts as a tool for space weather forecasting. *Comptes Rendus Physique*, *19*(1-2), 36-42.

49. Cane, H. V., Erickson, W. C., & Prestage, N. P. (2002). Solar flares, type III radio bursts, coronal mass ejections, and energetic particles. *Journal of Geophysical Research: Space Physics*, *107*(A10), SSH-14.

50. Lobzin, V. V., Cairns, I. H., Robinson, P. A., Steward, G., & Patterson, G. (2009). Automatic recognition of type III solar radio bursts: automated radio burst identification system method and first observations. *Space Weather*, *7*(4), 1-12.

51. Lobzin, V. V., Cairns, I. H., Robinson, P. A., Steward, G., & Patterson, G. (2010). Automatic recognition of coronal type II radio bursts: the automated radio burst identification system method and first observations. The Astrophysical Journal Letters, 710(1), L58.

52. Lobzin, V. V., Cairns, I. H., & Zaslavsky, A. (2014). Automatic recognition of type III solar radio bursts in STEREO/WAVES data for onboard real-time and archived data processing. Journal of Geophysical Research: Space Physics, 119(2), 742-750.

53. Salmane, H., Weber, R., Abed-Meraim, K., Klein, K. L., & Bonnin, X. (2018). A method for the automated detection of solar radio bursts in dynamic spectra. *Journal of Space Weather and Space Climate*, *8*, A43.

54. Cerruti, A. P., Kintner Jr, P. M., Gary, D. E., Mannucci, A. J., Meyer, R. F., Doherty, P., & Coster, A. J. (2008). Effect of intense December 2006 solar radio bursts on GPS receivers. Space weather, 6(10).

55. Luan, J., & Goldreich, P. (2014). Physical constraints on fast radio bursts. The Astrophysical Journal Letters, 785(2), L26.

56. Veronese, T. B., Rosa, R. R., Bolzan, M. J., Fernandes, F. R., Sawant, H. S., & Karlicky, M. (2011). Fluctuation analysis of solar radio bursts associated with geoeffective X-class flares. Journal of Atmospheric and Solar-Terrestrial Physics, 73(11-12), 1311-1316.

57. Bastian, T. S., Bookbinder, J., Dulk, G. A., & Davis, M. (1990). Dynamic spectra of radio bursts from flare stars. The Astrophysical Journal, 353, 265-273.

58. Burke-Spolaor, S., Bailes, M., Ekers, R., Macquart, J. P., & Crawford III, F. (2010). Radio bursts with extragalactic spectral characteristics show terrestrial origins. The Astrophysical Journal, 727(1), 18.

59. Kulkarni, S. R., Frail, D. A., Wieringa, M. H., Ekers, R. D., Sadler, E. M., Wark, R. M., ... & Bloom, J. S. (1998). Radio emission from the unusual supernova 1998bw and its association with the γ-ray burst of 25 April 1998. Nature, 395(6703), 663.

60. Afraimovich, E. L., Demyanov, V. V., Gavrilyuk, N. S., Ishin, A. B., & Smolkov, G. Y. (2009). Malfunction of satellite navigation systems GPS and GLONASS caused by powerful radio emission of the Sun during solar flares on December 6 and 13, 2006, and October 28, 2003. Cosmic Research, 47(2), 126-137.

61. Jones, J., & Richards, G. P. (2014, September). Automated recognition of type III solar radio bursts using mathematical morphology. In Advanced Maui Optical and Space Surveillance Technologies Conference.
62. Benz, A. O., & Wentzel, D. G. (1981). Coronal evolution and solar type I radio bursts-an ion-acoustic wave model. Astronomy and Astrophysics, 94, 100-108.
63. Zheleznyakov, V. V., & Zaitsev, V. V. (1968). The Origin of Type-V Solar Radio Bursts. Soviet Astronomy, 12, 14.
64. Stewart, R. T. (1965). Solar radio bursts of spectral type V. Australian Journal of Physics, 18(2), 143-166.

Appendix

Matlab source code

method 1 convolution

```
impath='C:\Users\User\Desktop\Msc Biomedicine
Computational and Computer
Science\ΠΤΥΧΙΑΚΗ\03A26_00.asg';
Iinit=I;
[N,M]=size(I);
figure; imshow(I,[])
nconv=11;
wv=15;    for iter=1:10

  S1=sum(I,2);
  S2=conv(S1,ones(1,nconv)/nconv);
  S2(1:(nconv-1)/2)=[];
  S2(end-(nconv-1)/2+1:end)=[];
  figure; plot(S1);
  hold on
  plot(S2,'k')

  idx=find(S1<0.999*S2);
  plot(idx,S1(idx),'om')
  xlabel('Image line index');
  legend('Sum of image values along lines','Smoothed
sum')

  I1=I;

  length(idx)
  NN(iter)=length(idx);
  for k=1:length(idx)
```

```
    lin=idx(k);
    if lin>wv & lin<N-wv
      for j=1:M
        a=I(lin-wv:lin+wv,j);
        I1(lin,j)=median(a);
      end
    end
  end

  figure; imshow(I1,[])
  hold on
  plot(ones(size(idx)),idx,'o')
  I=I1;
  drawnow
  if iter>3 & NN(iter)==NN(iter-1) & NN(iter)==NN(iter-2)
    break
  end
end
I=Iinit;
```

method 2 fft

```
impath='C:\Users\User\Desktop\Msc Biomedicine
Computational and Computer
Science\ΠΤΥΧΙΑΚΗ\03A28_1000.asg';
 [I,Nc]=load_image_fun(impath,1,500);
nw=35;
figure; imshow(I,[]);
II=fft2(I(1:630,1:Nc));
II=fft2(I);
[N,M]=size(I);
N2=N/2+1;
M2=M/2+1;
II2=fftshift(II);
figure; imshow(log10(1+abs((II2))),[]);
IImask=ones(N,M);
h=hanning(2*nw+1)';
for j=1:M
    IImask(N2-nw:N2+nw,j)=1-h.^4;
end
II3=ifft2(fftshift(II2.*(1-IImask)));
figure; imshow((II3),[])
figure; imshow(abs(1-IImask),[])
```

load image

```
fid=fopen('C:\Users\User\Desktop\Msc Biomedicine
Computational and Computer
Science\ΠΤΥΧΙΑΚΗ\03A26_0600.asg','rb')
n=(94412956)/6556;
CH1=[];
for i=1:2500
  ch1=[];
  ch2=[];
  for k=1:2
    head=fread(fid,256,'int8');
    ch1=[ch1,fread(fid,[630,5],'ubit16', 'ieee-be')];
    head=fread(fid,256,'uint8');
    ch2=[ch2,fread(fid,[630,5],'ubit16', 'ieee-be')];
  end

  CH1(:,i)=mean([ch1,ch2],2);
  CH2(:,i)=max([mean(ch1,2),mean(ch2,2)],[],2);
  CH2a(:,i)=max([ch1,ch2],[],2);
end
  figure; imagesc(CH1)
  xticklabels = 0:250:2500;
  xticks = linspace(1, size(CH1, 2), numel(xticklabels));
  set(gca, 'XTick', xticks, 'XTickLabel', xticklabels)
  xlabel('Time (x2 sec)')

  yticklabels = 650:-50:20;
  yticks = linspace(1, size(CH1, 1), numel(yticklabels));
  set(gca, 'YTick', yticks, 'YTickLabel', yticklabels)
  ylabel('Frequency (MHz)')
  figure; imagesc(CH2); title('2');
  figure; imagesc(CH2a); title('2a');
  figure; imshow(min(CH1(:))-CH1,[])
fclose(fid)

I=max(CH1(:))-CH1;
```

Read1

```
close all
clear all
fid=fopen('C:\Users\User\Desktop\artemis\asg,avg,act-
artemis\03A26_0600.asg','rb')
n=(94412956)/6556;
CH1=[];
for i=1:2500 % n
  head=fread(fid,256,'int8');
  ch1=fread(fid,[630,5],'ubit16', 'ieee-be');
```

```
  head=fread(fid,256,'uint8');
  ch2=fread(fid,[630,5],'ubit16', 'ieee-be');
  CH1(:,i)=mean([ch1,ch2],2);
end
  figure; imshow(CH1,[])
  figure; imshow(max(CH1(:))-CH1,[])
fclose(fid)

I=max(CH1(:))-CH1;
```

Read2

```
close all
clear all
fid=fopen('C:\Users\User\Desktop\ΠΤΥΧΙΑΚΗ\03A26_0600.asg'
,'rb')
n=(94412956)/6556;
CH1=[];
for i=1:2500 % n
  ch1=[];
  ch2=[];
  for k=1:2
    head=fread(fid,256,'int8');
    ch1=[ch1,fread(fid,[630,5],'ubit16', 'ieee-be')];
    head=fread(fid,256,'uint8');
    ch2=[ch2,fread(fid,[630,5],'ubit16', 'ieee-be')];
  end

  CH1(:,i)=mean([ch1,ch2],2);
  CH2(:,i)=max([mean(ch1,2),mean(ch2,2)],[],2);
  CH2a(:,i)=max([ch1,ch2],[],2);
end

  figure; imagesc(CH1)
  xticklabels = 0:250:2500;
  xticks = linspace(1, size(CH1, 2), numel(xticklabels));
  set(gca, 'XTick', xticks, 'XTickLabel', xticklabels)
  xlabel('Time (x2 sec)')

  yticklabels = 650:-50:20;
  yticks = linspace(1, size(CH1, 1), numel(yticklabels));
  set(gca, 'YTick', yticks, 'YTickLabel', yticklabels)
  ylabel('Frequency (MHz)')
  figure; imagesc(CH2); title('2');
  figure; imagesc(CH2a); title('2a');
```

```
  figure; imshow(min(CH1(:))-CH1,[])
fclose(fid)

I=max(CH1(:))-CH1;
```

Read3

```
I=imread('C:\Users\User\Desktop\Msc in Computer Science
and Computational Biomedicine\test1.bmp');
figure; imshow(I);
figure; plot(sum(I,2));
figure; plot(sum(rgb2gray(I),2));
help bwdilate
help imdilate
help strel
strel('line', 10, 45)
s=strel('line', 10, 45)
s.Neighborhood
s=strel('line', 7, 90)
s.Neighborhood
I1=imdilate(rgb2gray(I),s);
figure; imshow(I1);
Ig=rgb2gray(I);
figure; plot(Ig(93,:));
figure; plot(Ig(94,:));
figure; plot(Ig(98,:));
x=Ig(98,:);
X=fft(x);
X
X'
figure; plot(abs(X))
figure; plot(abs(fftshift(X)))
figure; plot(log10(1+abs(fftshift(X))))
x=Ig(93,:);
X=fft(x);
figure; plot(log10(1+abs(fftshift(X))))
x=Ig(156,:);
figure; plot(x)
g=fspecial('gaussian'
s=5;
g=fspecial('gaussian',[round(6*s)+1,1],s);
figure; plot(g)
sum(g)
format long
sum(g)
format
x1=conv(x,g','same');
x1=conv(double(x),g','same');
hold on;
plot(x1,'m');
```

Proc1

```
load im2.mat

[N,M]=size(I);
figure; imshow(I,[])

for iter=1:10

S1=sum(I,2);
S2=conv(S1,ones(1,11)/11);
S2(1:5)=[];
S2(end-4:end)=[];
figure; plot(S1);
hold on
plot(S2,'k')

idx=find(S1<0.95*S2);
plot(idx,S1(idx),'om')

I1=I;
wv=11;
for k=1:length(idx)
  lin=idx(k);
  if lin>wv & lin<N-wv
    for j=1:M
      a=I(lin-wv:lin+wv,j);
      I1(lin,j)=median(a);
    end
  end
end

figure; imshow(I1,[])
hold on
plot(ones(size(idx)),idx,'o')
I=I1;
end
```

proc1

```
[N,M]=size(I);
figure; imshow(I,[])

for iter=1:10
  S1=std(I(:,1:500),1,2);
  S2=medfilt1(S1,11);
  figure; plot(S1);
  hold on
  plot(S2,'k')
```

```
  idx=find(S1>1.05*S2);
  plot(idx,S1(idx),'om')

  I1=I;
  wv=11;
  for k=1:length(idx)
    lin=idx(k);
    if lin>wv & lin<N-wv
      for j=1:M
        a=I(lin-wv:lin+wv,j);
        I1(lin,j)=median(a);
      end
    end
  end

  figure; imshow(I1,[])
  hold on
  plot(M*ones(size(idx)),idx,'o')
  drawnow
  I=I1;
end
```

Proc2

```
clear all
load im2.mat
nw=35;
figure; imshow(I(1:630,1:630),[]);
II=fft2(I(1:630,1:630));
II=fft2(I);
[N,M]=size(I);
N2=N/2+1;
M2=M/2+1;
II2=fftshift(II);
figure; imshow(log10(1+abs((II2))),[]);
IImask=ones(N,M);
h=hanning(2*nw+1)';
for i=1:N
  if i~=N2
    IImask(i,M2-nw:M2+nw)=1-h.^4;
  end
end
II3=ifft2(fftshift(II2.*IImask));
Figure; imshow (abs (II3), [])
I=II3;
```